NTNU

Norwegian University of
Science and Technology

Experimental Studies of Finger and Fracture Instabilities in Clays Throughout the Sol-Gel Transition

Beate Ulrikke Krefting Cappelen

Master of Science in Physics and Mathematics
Submission date: June 2011
Supervisor: Jon Otto Fossum, IFY

Norwegian University of Science and Technology
Department of Physics

Abstract

This thesis concerns studies of fingering and fracturing in two different clay suspensions. The aim of this thesis is to identify how the phenomena of fingering transitions into fracturing as the breaking medium gradually becomes more solid-like, and to study fingering and fracturing using crossed polarizers to see the nematic phase of Laponite clay suspension.

A solution of 3 wt% Laponite RD suspended in distilled water was studied in a Physica MCR300 Rheometer to find when the sol-gel transition state occured. The conditions in the rheometer and the conditions in the Hele-Shaw cell are so different, that the results from the rheometer could not be transferred and used in the experiments in the Hele-Shaw cell.

Experiments have been performed in two different setups, both in a linear Hele-Shaw cell (setup I) and in a radial Hele-Shaw cell (setup II). During the experiments, two different clay suspensions have been used: Laponite clay suspension and Bentonite clay suspension. The Laponite clay suspension consists of 3 wt% or 3,5 wt% Laponite and distilled water, and is used in setup I. The Bentonite clay suspension consists of 8, 9 or 10 wt% Bentonite and distilled water, and is used in setup II. Experiments have been performed using different velocities to the pistons which pull the clay apart, to see if the velocity has an influence on the shape of the finger/fracture. The velocities used in this thesis are 1, 5, 10, 20 and 30 mm/s for the liquid state, 1, 5 and 10 mm/s at the sol-gel transition state and 1 and 5 mm/s for the gel state. The clay suspensions are left for different amount of time in the Hele-Shaw cells to achieve different states to the suspensions. Doing this, it is possible to see how the fingers gradually becomes fractures. Experiments are done in the liquid state, at the sol-gel transition state and in the gel state of the clay suspensions. It was found that the finger width decreased with the age to the clay suspension in the liquid state, but it stayed constant at different velocities of the pistons. In the gel state, the fracture experiments were not so good, since there were problems with air leakage when the suspension stayed in the Hele-Shaw cell for an amount of time longer than 1 day. The experiments performed during the sol-gel transition state gave good results. It was found by doing experiments that the sol-gel transition state occurred

after around 1 day for Laponite clay suspension with a concentration of 3,5 wt% Laponite. Here, as well as in the liquid state, the shape of the finger did not change with the velocity of the pistons, but with the age and concentration of the clay suspension.

Experiments using setup II did not give good results. The bad results were caused by air leakage in the cell, and several other problems too great to be dealt with. This resulted in experiments using setup II being stopped, and experiments only being performed in setup I with and without crossed polarizers.

In setup I, experiments have also been done using crossed polarizers. This is done by placing the Hele-Shaw cell between two polarizers that have their transmission axis perpendicular to each other. The experiments with the crossed polarizers are performed using different ages of the clay suspension, and with different velocities to the pistons. Experiments in the liquid state, using crossed polarizers were not different from the experiments in the liquid state without crossed polarizers. Experiments performed in the gel state of the Laponite clay suspension showed the nematic state of the suspension. The nematic ordering did not change from 1 day to 3 days.

Contents

List of Figures

Preface

This thesis is a result of the work performed during the tenth semester of my Master's degree in Applied Physics and Mathematics at the University of Science and Technology (NTNU). This work is a continuation of the work performed on the project thesis during the ninth semester. The work has been carried out at the Complex Systems and Soft Materials Group (Complex) at the Department of Physics at NTNU.

I am really grateful that I got the opportunity to go to CEA in Paris for one week to work with Elisabeth Bouchaud and Baudouin Saintyves. It was really helpful to see their setup, which is similar to my setup at NTNU. It was interesting to follow their experiments and to profit from their results. They gave me a lot of inspiration and insight into the world of fingering and fracturing.

I would like to thank my supervisor Professor Jon Otto Fossum for help and guidance throughout the semester. Elisabeth Bouchaud and Baudouin Saintyves have been very helpful, giving me advises, guiding me through my experiments and being open to answer every question I had. I would like to thank our technician Ole Tore Buseth for all his help with the technical problems I had during the semester and Zbigniew Rozynek for the help with the rheometer. In the end I would like to thank my fellow student Christoffer Berge Hansen for helping me make the bubble remover device.

Trondheim, 17.06.2011 Beate Krefting Cappelen

Chapter 1

Introduction

Ideal solids deform elastically, the energy required for the deformation is fully recovered when the stresses are removed. Ideal fluids such as liquids and gases deform irreversibly - they flow. The energy required for the deformation is dissipated within the fluid in the form of heat and cannot be recovered simply by removing the stresses. There are very few liquids that can be classified as ideal fluids. Most fluids lie in the region somewhere between liquid and solid, they inhibit both viscous and elastic behavior, and are named *visco-elastic*. This can be further extended by the introduction of the time-scale of any deformation process. It is written in the bible that: "Everything flows, if you wait long enough, even mountains ..." [1]

An example of this is in old glass windows. When they were made, they were of uniform thickness, but as time goes by the glass molecules have flown under the influence of gravity. This results in the thickness at the top of the glass windows decreases, while the thickness has increased at the bottom. Thus, even though glass seams really solid, it still belongs to the group of fluids if you wait long enough. One can conclude from this that materials such as glass or water cannot be classified as liquids or solids, but as materials exhibiting a liquid or solid behavior under certain conditions of stress, shear rates or time [1].

Pattern formation has been studied for fundamental reasons, but also because the need of industrial research. For instance the petroleum industry

has been consistently trying to find ways of inhibiting viscous fingering[1], because it limits oil recovery in porous media. When a new well is drilled, oil flows out of it spontaneously. When this stops, most of the oil is still absorbed in porous rocks. If several wells are drilled next to each other, one can try to force the oil to flow from one of them by injecting water with high pressure into the others. A problem here is that water is less viscous than oil, such that the front is unstable and fingers of water will rapidly reach the extraction well and short-circuit the motion of the oil [2].

Another situation can be with extraction of oil from a crude oil reservoir located in the pores of sedimentary rock. A newly tapped deposit is held under earth pressure which will drive a portion of the oil to the receiving bore holes. When this fails, pumping of water down holes set in a ring around the field is started. The water sweeps crude before it, the water/oil interface is unstable, and fingering is observed. When the water bypasses the oil in the form of fingers, the water reaches the receiving well first. Oil wells which have been abandoned because of fingering may still contain as much as 50% of the original deposit. Hence, enhanced oil recovery is important [3].

Viscous instabilities can also be a factor in coating processes, where a fluid has to be spread evenly onto a solid surface, or if one wants to obtain a good metal plating trying to avoid any fractal or dendritic growth in electrodeposition. These instabilities can be both crucial and beneficial [2].

Pattern formations as fractures have also been investigated thoroughly by a number of scientists. Fractures are important because unstable crack propagation, such as earthquakes, can produce catastrophic failure with the probability of loss of lives and properties. The problem is difficult because of the singularity in the strain and stress field at the crack tip, giving rise to nonlinear behavior at the tip. The problem is even further complicated by a host of environmental factors which affect the growth and initiation of the fracture [4].

In 1898 Henry Selby Hele-Shaw introduced a simple system to study the flow of water around various objects. The cell he designed consisted of two parallel transparent plates separated of a relatively small gap of hight b. The

[1] Viscous fingering will be discussed in section 3.4.1

viscous fluids were placed between the plates, and the pressure could be applied either in one of the edges of the cell (the linear version) or at the center of the upper plate of the cell (the radial version). This cell was designed for the study of a two-dimensional flow, and was called a *Hele-Shaw cell* after Henry Selby Hele-Shaw [5]. Figure 1.1 illustrates the principle of a linear and a radial Hele-Shaw cell.

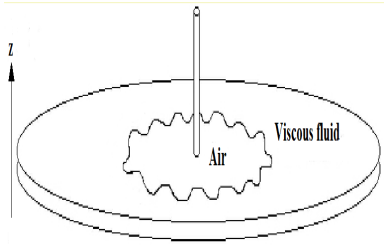

(a) *Sketch showing a radial Hele-Shaw cell. Figure adapted from [6].*

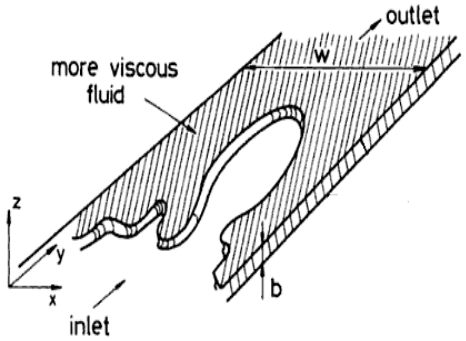

(b) *Sketch showing a linear Hele-Shaw cell. Figure adapted from [5].*

Figure 1.1: *Sketches of a radial, and a linear Hele-Shaw cell.*

Saffman and Taylor were some of the first to study viscous fingering in a linear Hele-Shaw cell in 1958 [7]. They did experiments where a viscous fluid confined between closely spaced parallel sheets of glass, was driven out by a less viscous fluid. These experiments showed that single fingers could be produced as seen in figure 1.2

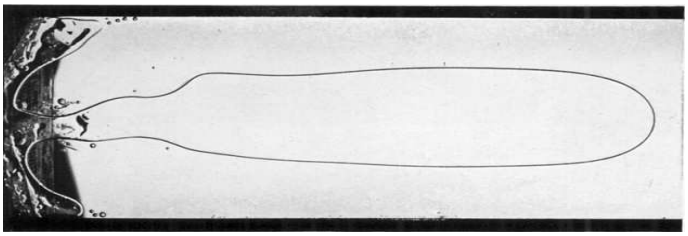

Figure 1.2: *Picture showing an air finger advancing into glycerine in a Hele-Shaw cell. Experiment performed by Saffman and Taylor [7].*

Chapter 2 gives a short introduction to clay and a description of the physical structure of clays. It goes deeper into the physical properties of the clays Laponite and Bentonite. Section 2.2 gives a description of colloidal dispersions, and it describes both Laponite and Bentonite as colloidal dispersions.

In chapter 3 the theory needed for this thesis is summarized. Section 3.1 and 3.2 talks about rheology and rheometry. It goes deeper into the expression *viscoelasticity*, and it also summarizes the material properties shear-thinning, shear-thickening, thixotropy, anti-thixotropy and bingham plastics. Linear viscoelasticity and oscillatory shear is thoroughly discussed. Section 3.3 contains linear fracture mechanics. It gives the conditions for crack propagation and it shows the three different modes for crack propagation. Section 3.4 summarizes fingering and fracturing in Hele-Shaw cells. This section gives a description of a Hele-Shaw cell, and it explains the difference between radial and linear Hele-Shaw cells. It gives the difference between viscous fingering and viscoelastic fracturing. Section 3.5 explains the sol-gel transition, when and why it occurs using the perlocation theory. Section 3.6 take liquid crystals into account, discusses the different phases of liquid crystals, and goes deeper into the nematic phase. The last section, section 3.7, summarizes polarization, polarizers and birefringence.

Chapter 4 summarizes the experimental part. It explains the preparation of the samples, and it shows the setup both in a linear cell (setup I with and without crossed polarizers) and in a radial cell (setup II). Chapter 4 also give a description of the rheological measurements performed in this thesis. Chapter 5 gives the results from the setups and from the rheological measurements, and discusses the results.

Chapter 6 is the last chapter, and gives the conclusion and future studies. Both studies that I imagine would be wise to perform to get better results, and studies which I would have performed if I have had enough time.

Chapter 2

Clay samples

2.1 Clay

Clays are present almost everywhere on Earth, they are abundant, inexpensive and environment friendly. Most of the natural clays are very heterogeneous mixtures of minerals, however, pure clays can now be made synthetically. Clays are composed of extremely fine, usually plate-shaped crystal layers typically with diameters less than 2 μm and less then a few nm thick [8].

Clays have the unique ability to be pillared by intercalated guest ions, making their study of fundamental importance within the general context of "nanosandwiches" as a basis for nanotechnologies. The small particle size and microporous structure of clays give them their extremely important capability to absorb water and become *hydrated clays* [8].

Most clays are hydrous silicates of Al, Mg, Fe and other elements, and go under the name *phyllosilicates*. Phyllosilicates ideally contain a continuous tetrahedral sheet. Each tetrahedron consists of a cation, coordinated to four oxygen atoms, and linked to adjacent tetrahedra by sharing three corners to form a two-dimensional hexagonal structure illustrated in figure 2.1a. In the octahedral sheet, connections between each octahedron to neighboring octahedra are made by sharing edges. The edge-shared octahedra form sheets of hexagonal symmetry [9] as illustrated in figure 2.1b. The 1:1 layer structure consists of the repetition of one tetrahedral and one octahedral sheet, and in

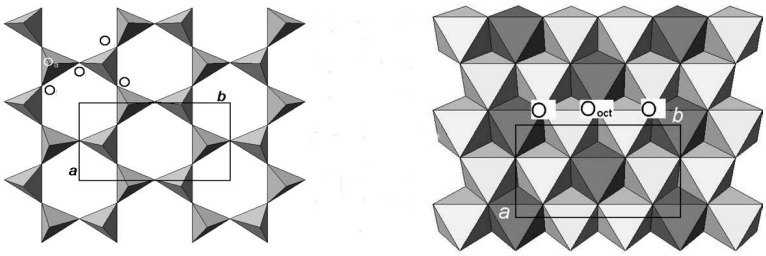

(a) *A tetrahedral sheet.* (b) *An octahedral sheet.*

Figure 2.1: *Tetrahedral and octahedral sheets seen from above. O denotes oxygen atoms. a and b refer to unit-cell parameters. Figure adapted from [9].*

the 2:1 layer structure one octahedral sheet is sandwiched between two tetrahedral sheets as illustrated in figure 2.2. The thickness of the fundamental sheet for the 2:1 structure is about 10 Å.

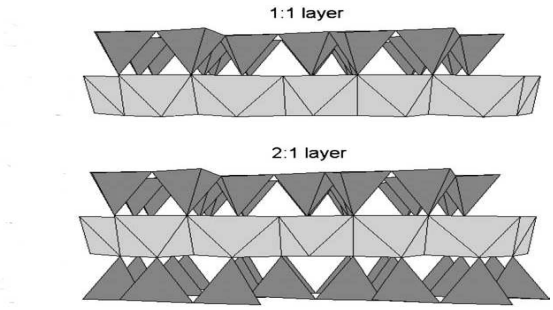

Figure 2.2: *The structure of 1:1 and 2:1 layered phyllosilicates. Figure adapted from [9].*

2.1.1 Laponite

Laponite is a synthetic magnesium silicate clay with general formula $Na^{+0.7}[Si_8Mg_{5.5}Li_{0.3}H_4O_{24}]^{-0.7}$, diameter around 25 nm and a thickness of 1 nm [10]. Each Laponite particle is a three layer silicate composed of a central octahedrally coordinated magnesium-oxygen-hydroxide sandwiched between

two tetrahedrally coordinated silica-oxygen sheets [11]. A Laponite particle and its crystallographic structure is shown in figure 2.3. Laponite is a synthetic hectorite-type smectite, with a bulk density of $\rho_L = 2.65$ g/cm^3 [11], and has a trioctahedral character. Laponite is principally used as fillers and thickening agents for aqueous preparations. In the smectite 2:1 phyllosilicates the layer is usually negatively charged, with a charge between 0.2 and 0.6 per half unit cell [9]. The low charge in smectites allows hydrated ions and polar ions to be intercalated between the layers. Except for the layer charge and hydration of the interlayer cation, the structure of smectites is similar to that of other 2:1 phyllosilicates.

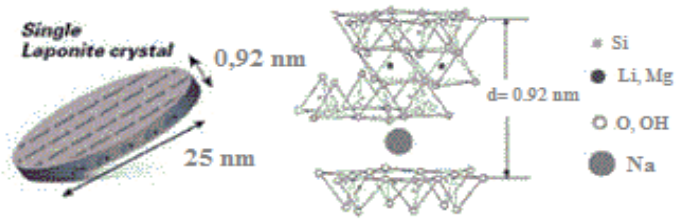

Figure 2.3: *Characteristic shape, dimensions, crystallographic structure and chemical formula for a Laponite particle. Figure adapted from [10].*

Laponite has a high chemical purity and its elementary particles have small anisotropy compared to other natural clay materials. Laponite RD with the chemical formula ($Si_8Mg_{5.45}Li_{0.4}H_4O_{24}Na_{0.7}$), is dispersed in water as individual plate-like sheets having a thickness of 10 Å and an average diameter close to 300 Å. These particles bear a structural negative charge that is balanced by Na+ counterions located all around the microcrystalline particles [12, 13].

There exists several Laponite grades and characteristics, which are depicted in table 2.1. Laponite RD is used in the experiments in this report. Laponite dispersions are very sensitive to pH, for $pH < 9$ Laponite RD particles dissolve. Prior studies on Laponite RD [14] showed that the Laponite RD dispersions are stable at pH = 10.

Table 2.1: *Summary of Laponite grades and characteristics, adapted from [15].*

Gel forming grades	Sol forming grades	Function
RD	RDS	Rapid dispersion in water for general and industrial use
XLG	XLS	Rapid dispersion in water, high purity, low heavy metal content for personal care/cosmetic applications
D,DF	DS	Rapid dispersion in sorbitol solution for toothpaste applications
	S,JS	High sol stability grades for electrically conductive, antistatic and barrier films

2.1.2 Bentonite

Bentonite has its origin in volcanic rock alteration or authigenic. It is an impure clay and its main clay minerals constituents is Montmorillonite [9]. Montmorillonite is in the Smectite group, and has a dioctahedral character. Smectites have particles of colloidal size and have a high degree of layer stacking disorder. Smectites also have a high specific surface area, and a moderate layer charge. Montmorillonite has the same layer charge as Laponite, ~ 0.2 - 0.6 charge per formula unit. The chemical formula of Montmorillonite is $Si_8Al_{3.5}Mg_{0.5}O_{20}(OH)_4$ [9].

Bentonite is the most important component of a water-based drilling fluid. The main reason to use Bentonite in drilling fluids is to increase the viscosity of the drilling fluid and to reduce the filtration loss [16]. Bentonite can also be added to paints, pesticide formulations, cosmetical and pharmaceutical preparations [17].

An overview of the structure to montmorillonite is shown in figure 2.6. At a macroscopical level, the Bentonite particles are anisotropic single crystal sheets. The thickness of the sheets is approximately 1 nm, whereas the size

in the a,b plane is close to the order of 500 nm [18].

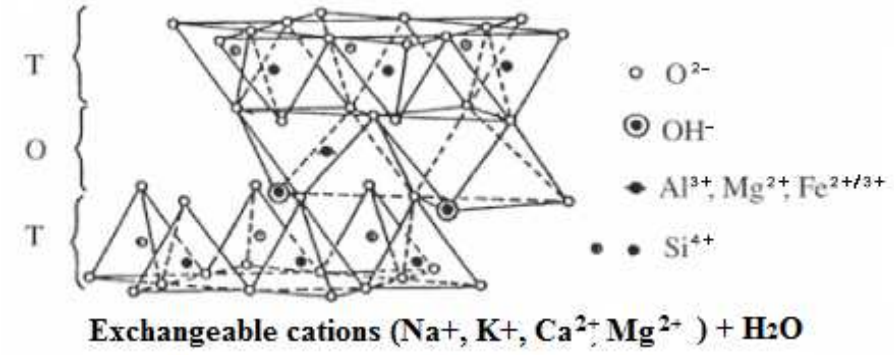

Figure 2.4: *Montmorillonite structure. T:Tetrahedral sheet, O:Octahedral sheet. The figure is adapted from [19].*

2.2 Colloidal dispersions

Colloidal materials can show themselves in a wide variety of physical phases. They can form weakly non-newtonian fluids[1] when stabilized as dilute suspensions in simple liquids. At higher concentrations they can often form viscoelastic, shear-thinning[2] pastes, and at even higher concentrations they can form physical gels. If all the dispersion liquid is removed, they can form coherent and fragile solids [18]. The dispersion can be a sol, i.e., the particles form a stable colloidal dispersion, or is coagulated, flocculated or thickened forming a gel [17].

A colloid is a substance microscopically dispersed evenly throughout another substance. Particle sizes in colloidal systems generally range from 1 nm to 10 μm. For many dispersions, the physical behavior can change dramatically with small differences in composition. This behavior is a result from the different forces that act among the particles [20]. In an unstable colloidal dispersion particles can aggregate and then flocculate due to the inter-particle attraction, if the gravitational forces overcome the *Brownian forces* that work

[1]Non-newtonian fluids will be discussed in section 3.1

[2]Shear-thinning materials will be discussed in section 3.1.1

to keep the particles suspended and hinder sedimentation [9].

Colloidal dispersions are abundant, and can be found everywhere around us. They can exists in different combinations of liquid, gas and solid state. Examples of colloidal dispersions can be milk (liquid particles dispersed in liquid), fog or mist (liquid particles dispersed in gas) or smoke (solid particles dispersed in gas).

2.2.1 Colloidal dispersion of Laponite

Smectites have exceptional water absorption characteristics. Smectites are able to absorb up to half of their mass in water. When Laponite powder is dispersed in water, it is first white and non-transparent, then after being stirred for a while it becomes transparent. This happens because the platelets in the Laponite clay have been delaminated (Figure 2.5) into individual silicate layers and is too small to be seen with the bare eye, but can be seen by for example Transmission Electron Microscopy (TEM) or X-ray techniques. The single silicate layers are surrounded by a few water layers that move with the particles. It is very likely that at least two layers of water remain attached to the particles [9].

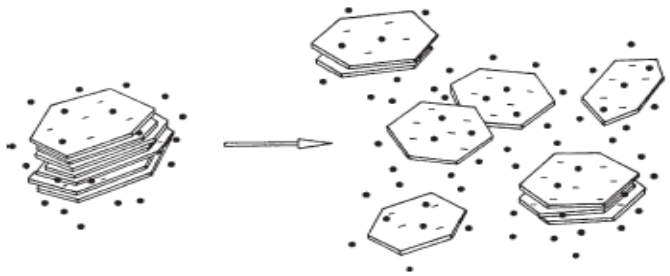

Figure 2.5: *Delamination of smectite particles in aqueous dispersions. The figure is adapted from [9].*

2.2.2 Colloidal dispersion of Bentonite

Colloidally dispersed Bentonites are thickening and thixotropic[3] agents. Colloidal Bentonite dispersions are only obtained in the presence of amounts of sodium ions corresponding to the cation exchange capacity [17].

When Bentonite powder is dispersed in water, water enters the interlayer space in the montmorillonite and hydrates both the cations and the internal surfaces with different amounts of water layers. This results in a swelling of the crystalline. Crystalline swelling is a result of water molecules gradually shielding the attractive interaction between cations and internal surfaces as the humidity increases [21]. This is illustrated in figure 2.6.

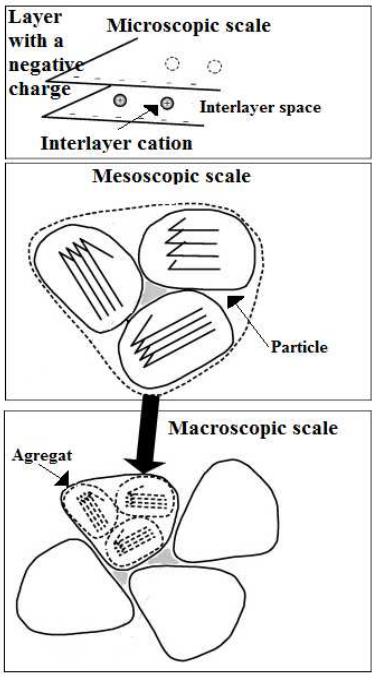

(a) *A representation of the structure of montmorillonite.*

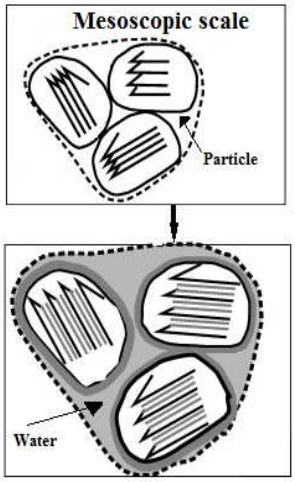

(b) *Schematic view for hydration of montmorillonite.*

Figure 2.6: *Hydration of montmorillonite. Figures adapted from [21].*

[3]Thixotropy will be discussed in section 3.1.1

2.2.3 The colloidal contribution to viscosity

Overall repulsion between the particles of a suspension is created if the particles carry electrostatic charges of the same sign. For flow to occur, particles have to be forced out of their equilibrium positions to flow against the electric fields of the neighboring particles into nearby vacancies in the imperfect lattice. At very high shear rates, two dimensional layering occurs, the electrostatic contribution loses its dominance and the viscosity decreases [3].

The formation of flocs leads to a bigger effective phase volume than that of the primary particles. This results in an additional increase in the viscosity that exceeds the expected viscosity from the phase volume of the individual particles. Flocs have the possibility of forming chains which form networks throughout the liquid. All flocculated structures take time to break down and rebuild, and are therefore associated with thixotropic behavior[4]. Brownian motion is the driving force to rebuild the floc, and since this increases with a decrease in particle size, the rate of thixotropic change is a function of particle size. Flocculated systems usually have high viscosities at low share rate, and are very shear-thinning. In many cases the Bingham model[5] has been used to describe their behavior [3].

[4]Thixotropic behavior will be discussed in the section 3.1.1
[5]Bingham plastics will be discussed in the section 3.1.1

Chapter 3

Theory

3.1 Rheology

The term "Rheology" was invented by Professor Bingham of Lafayette College, Indiana. It means *The study of the deformation and flow of matter* [3]. Materials that can be studied are of widely differing materials as asphalt, lubricants, paints, plastics and rubber. Significant advances have also been made in biorheology, in polymer rheology and in suspension rheology.

An important parameter in rheology is *viscosity*, or "internal friction" which is a measure of "resistance to flow". The constant of proportionality η is called the coefficient of viscosity, i.e.

$$\sigma = \frac{\eta U}{d} \tag{3.1}$$

where σ is the force per unit area denoted as F/A, required to produce the motion and is proportional to the "velocity gradient" or "shear rate" U/d. It is usual to write $\dot{\gamma}$ for the shear rate [3].

Sir Isaac Newton was the first to introduce the concept of viscosity, and fluids with a variable value of viscosity at constant temperature are commonly known as non-Newtonian fluids. Newtonian fluids such as e.g. water and "common" liquids, have a constant viscosity at fixed temperatures. Newtonian fluids follow *Navier-Stokes* equation [3].

If Newtonian viscous liquids are one extreme, the other extreme would be *Hookean elastic solids*. In the case of a Newtonian liquid, the flow persists as long as the stress is applied, but does not recover its original shape after removing the stress. In contrast, for a Hookean solid, a shear stress σ applied to the upper surface with an area A and a fixed bottom face, results in an instantaneous deformation. This is shown in figure 3.1. The deformed state persists as long as the stress is applied. When removing the shear stress the original shape of the solid is recovered. The shear stress is given as [3]

$$\sigma = \frac{F}{A} = G\gamma \tag{3.2}$$

where G is the shear modulus, or "rigidity modulus", and γ is the shear angle.

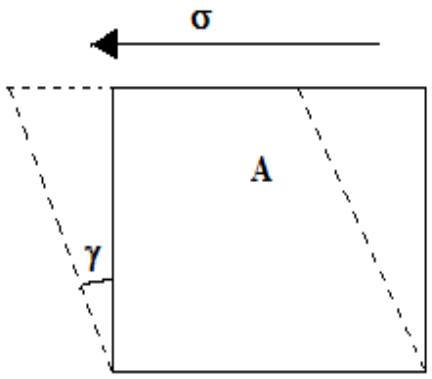

Figure 3.1: *Illustration of an applied stress to a Hookean solid at the upper surface, with the bottom face fixed. This leads to a deformation defined by the shear angle.*

While solids and liquids react very differently to stresses, there are no basic differences in the rheology to liquids and *gases*. Gases just have a significant lower viscosity than liquids, for example the viscosity of hydrogen gas at 20 $^{\circ}C$ is a hundredth of the viscosity of water. The difference between liquids and gases is that their viscosities are inversely dependent on temperature [1].

There are materials that cannot be described with either Hook's law for solids, or by Newton's law for liquids alone. These are solid-like materials that have elements of flow in the deformation pattern. Such behavior can be described as *viscoelasticity*. The two extremes explained over are viewed as being outside the scope of rheology. The over-riding concern is therefore with materials between these classical extremes [3]. Viscoelastic fluids are characterized by exhibiting both viscous and elastic characteristics when undergoing deformation and are called *Maxwell fluids* [22]. The different rheological properties of different materials are shown in table 3.1

Table 3.1: *Properties of different materials.*

Viscous	Viscoelastic	Viscoelastic	Elastic
Ideally viscous liquids	Viscoelastic liquids	viscoelastic solids	Ideally elastic solids
Water, oils	Glues, shampoos	Gels, rubbers	Steel, stone
Follow Newton's laws			Follow Hooke's law

3.1.1 Non-linearity

The elastic and viscous behaviors in terms of the laws of Hooke and Newton are examples of linear laws. They assume direct proportionality between stress and strain, or strain rate. However, the range of stress over which materials behave linearly is very limited. Material properties such as rigidity modulus and viscosity can change with the applied stress, and the stress do not need to be high. The change can occur either instantaneously or over a long period of time, it can appear as either an increase or a decrease of the material parameter, and is non-linear behavior [3]. In this section examples of non-linearity are summarized.

Shear-thinning materials

A **decrease** of the material parameter is called *shear-thinning* (also called pseudoplastic). When there is an increase in the rate of shear in steady flow, there is a reduction of the viscosity. Examples of shear-thinning fluids are mayonnaise, toothpaste, dispersions, suspensions etc. It holds its shape under the influence of gravity, but starts to flow for applied stresses, such as squeezing on a tube. Fluids like these, which do not flow unless they are subject to a certain load, are called yield stress fluids. They behave as solids for small applied stresses, and as liquids for high stresses [3]. There can be several reasons for these behaviors. Liquid products usually consist of different components. There can be rod-like particles as in clay dispersed in a liquid, there can be entangled molecular chains in polymers solutions or droplets of one liquid dispersed in another liquid. With increasing shear rates the rods can be turned lengthwise in the direction of the flow, the entangled chains can be disentangled (stretched out) and oriented in the direction of the flow or the droplets can be squeezed into the shape of "rugby balls" [1]. Examples of these situations are illustrated in figure 3.2.

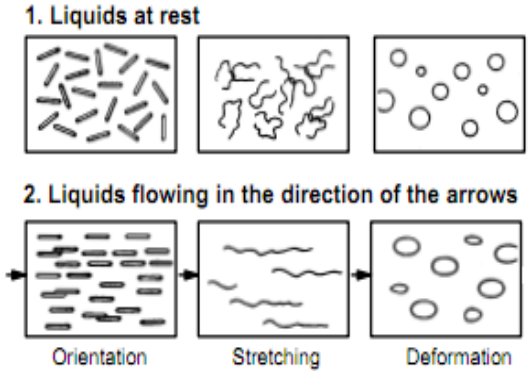

Figure 3.2: *Dispersions at rest and flowing through a tube. Figure adapted from [1].*

Another possible reason for shear-thinning can be that solvent layers are stripped from dissolved molecules or from particles, which means, that the intermolecular interactions causing resistance to flow become reduced [1].

Shear-thickening

If there is an **increase** of the material parameter, then it is called *shear-thickening* (also called dilatant flow behavior). This effect occurs when particles are densely packed, and the amount of liquid is sufficient to fill the gaps between the particles. At rest and at low shear rates, the suspension behaves as a liquid and the dilatant flows easily. At higher shear rates, the liquid is unable to fill the gaps between the particles, friction increases, causing the viscosity to increase [1]. An example of this is a mixture of cornstarch and water. At rest the mixture behaves as a liquid, but at high shear rates it becomes very solid like.

Thixotropy and anti-thixotropy

Thixotropy and anti-thixotropy are time dependent effects. Thixotropy is a decrease of the apparent viscosity with time at a constant rate of shear, followed by a gradual recovery when the motion is stopped. While anti-thixotropy is an increase of the apparent viscosity with time [3]. Thixotropy usually occurs in circumstances where the liquid is shear-thinning, and likewise anti-thixotropy usually occurs in circumstances where the liquid is shear-thickening.

In shear-thinning liquids, the liquid becomes thinner when the shear is increased due to the particle/molecular orientation in the direction of flow surpassing effect of the Brownian movement of molecules. This orientation is again lost just as fast as orientation came about in the first place. Many dispersions show similar change in viscosity with both an increase and a decrease in shear. It is typical for many dispersions that they also show this potential for a time-related particle-interaction. This will lead to bonds creating a three-dimensional network structure, which is often called a gel. These bonds are relatively weak. They break easily when the dispersions is subjected to shear over an extended period of time. When the network is broken, the viscosity drops with time to a lowest possible level, and can be described as a "sol[1]" [1].

A thixotropic liquid is defined as having the potential to rebuild its gel-structure, when the substance is allowed to rest for a certain period of time.

[1] A definition of a sol is given in section 3.5

The change of a gel to a sol, and of a sol to a gel is reproducible any number of times. An example of a thixotropic material is non-dripping paint. When brushing paint onto a vertical wall, it breaks down its thixotropic structure and allows it to be spread thinly and easily. Once applied to the wall the paint must recover its gel structure as fast as possible to prevent the paint layer from sagging off the wall. An anti-thixotropic liquid will have an increase in viscosity when exposed to a shear, and again a decrease in viscosity when left at rest for an extended period of time [1]. Anti-thixotropic behavior can be explained as time dependent dilatant behavior.

Bingham plastics

A Bingham plastic is a plastic that will not flow until a critical yield stress is exceeded, also the viscosity is infinite at zero shear rate [3]. It describes shear-thinning liquids that additionally feature a yield point. Bingham plastics together with shear-thinning and shear-thickening materials are time-*independent*. Flow curves for time-independent fluids are given in figure 3.3.

Plastic fluids are dispersions, which at rest, can build up an interparticle network of binding forces. These forces give the substance a solid character with an infinitely high viscosity. Only when the outside forces are strong enough to overcome the network forces, surpass the threshold shear stress called the yield point, does the network collapse. Volume elements can now change positions irreversibly: the solid turns into a flowing liquid. Examples of Bingham plastics are greases, lipstick masses and oil well drilling fluids [1].

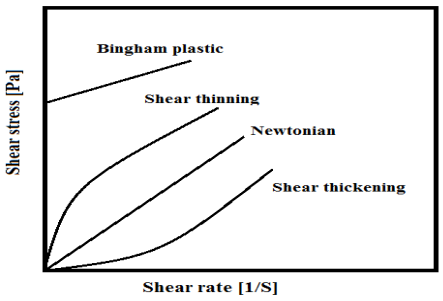

Figure 3.3: *Flow curves for time-independent fluids, shown as shear rate as a function of share stress. Figure adapted from [23].*

3.1.2 Linear viscoelasticity

The development of the mathematical theory of linear viscoelasticity is based on a *superposition principle*. This implies that the response (e.g. strain) is proportional to the value of the initiating signal (e.g. stress). The general differential equation for linear viscoelasticity can be written as [3]:

$$(1+\alpha_1\frac{\delta}{\delta t}+\alpha_2\frac{\delta}{\delta t^2}+...+\alpha_n\frac{\delta}{\delta t^n})\sigma = (\beta_0+\beta_1\frac{\delta}{\delta t}+\beta_2\frac{\delta^2}{\delta t^2}+...+\beta_m\frac{\delta^m}{\delta t^m})\gamma \quad (3.3)$$

Where σ denotes shear stress and γ denotes strain. Now some special cases of equation 3.3 are considered. If both β_0 (=G) and $\beta_1(=\eta)$ are the only non-zero parameters, we have

$$\sigma = G\gamma + \eta\gamma' \quad (3.4)$$

Which is one of the simplest models of viscoelasticity, and is called the *Kelvin model*. Another simple model is the *Maxwell model*. Here α_1 and β_1 are the only non-zero material parameters, so that [3]

$$\sigma + \tau_M\sigma' = \eta\gamma' \quad (3.5)$$

Where $\alpha_1 = \tau_M$ and $\beta_1 = \eta$. The rate constant τ_M is called the *relaxation time*.

The generalized Maxwell model may have a finite number or an enumerable infinity of Maxwell elements, each with a different relaxation time. To generalize from an enumerable infinity to a continuous distribution of relaxation times, the simple Maxwell model, whose behavior is characterized by equation 3.5 or what is equivalent

$$\sigma(t) = \frac{\eta}{\tau}\int_{\infty}^{t}\exp\left[-(t-t')/\tau\right]\gamma'(t')dt' \quad (3.6)$$

Then consider a number, n, of discrete Maxwell elements. Then using the superposition principle:

$$\sigma(t) = \sum_{i=1}^{n}\frac{\eta_i}{\tau_i}\int_{-\infty}^{t}\exp\left[-(t-t')/\tau_i\right]\gamma'(t')dt' \quad (3.7)$$

$N(\tau)$ is now introduced as the contribution to the total viscosity of all the Maxwell elements with relaxation times lying between τ and $\tau+d\tau$. Equation 3.7 can then be rewritten to

$$\sigma(t) = \int_0^\infty \frac{N(\tau)}{\tau} \int_{-\infty}^{t} \exp\left[-(t-t')/\tau\right]\gamma'(t')dt'd\tau \tag{3.8}$$

A *relaxation function* ϕ is defined by:

$$\phi(t-t') = \int_0^\infty \frac{N(\tau)}{\tau} \exp\left[-(t-t')/\tau\right]d\tau \tag{3.9}$$

And equation 3.8 can finally be written as [3]:

$$\sigma(t) = \int_{-\infty}^{t} \phi(t-t')\gamma'(t')dt' \tag{3.10}$$

Oscillatory shear

The response of viscoelastic materials to a small-amplitude oscillatory shear is studied for investigating linear viscoelastic behavior. First let [3]:

$$\gamma(t') = \gamma_0 \exp\left(i\omega t'\right) \tag{3.11}$$

Where ω is the frequency and γ_0 is a strain amplitude. The complex quantity $\exp\left(i\omega t'\right)$ represents oscillatory motion. Then if this is substituted into the integral equation 3.12, it is obtained

$$\sigma(t) = i\omega\gamma_0 \exp\left(i\omega t\right) \int_0^\infty \phi(t-t') \exp\left(-i\omega(t-t')\right)d(t-t') \tag{3.12}$$

In oscillatory shear we define a *complex shear modulus* $G*$ [3]:

$$\sigma(t) = G*(\omega)\gamma(t) \tag{3.13}$$

And one can write

$$G* = G' + iG'' \tag{3.14}$$

G' and G'' are referred to as the *storage modulus* (elastic behavior) and *loss modulus* (viscous behavior) respectively. G' is also called the dynamic

rigidity. If the special case of the Maxwell model is considered, given by equation 3.5 (with $\tau_M = \tau$) it can be shown that [3]:

$$G* = \frac{i\omega\eta}{1 + i\omega\tau} \tag{3.15}$$

$$G' = \frac{\eta\tau\omega^2}{1 + \omega^2\tau^2} \tag{3.16}$$

$$G'' = \frac{\eta\omega}{1 + \omega^2\tau^2} \tag{3.17}$$

A method of characterizing linear viscoelastic response is to plot G' and the *loss angle* δ. δ is given as [3]:

$$\tan\delta = \frac{G''}{G'} \tag{3.18}$$

Table 3.2 shows how the viscoelastic behavior changes with G', G'' and δ.

Table 3.2: Viscoelastic behavior at different G' and G''

$G'' > G'$	$G'' = G'$	$G' > G''$
Liquid-like structure	"At the gel point"	Gel-like structure
Viscous	**Viscoelastic**	**Elastic**
$\tan\delta > 1$	$\tan\delta = 1$	$\tan\delta < 1$

3.2 Rheometry

A rheometer is an instrument for measuring rheological properties in solids, semi-solids and fluids. The rheometer relies on rotational motion to achieve a simple shearing flow [3]. To do this, the rotor rotates while the cylinder is stationary as seen in figure 3.4. The rotor is driven by a motor with defined torque values, leading to a laminar flow. The resistance of the sample placed against the applied torque or shear stress will allow the rotor to rotate only at a speed, denoted as the *shear rate*, inversely correlating to the viscosity of the sample [1].

The storage and loss modulus can be calculated using the equations [1]:

$$\eta' = G''/\omega \tag{3.19}$$

$$\eta'' = G'/\omega \tag{3.20}$$

Where $\omega = 2\pi f$ is the frequency of the rotor, and η' is the dynamic viscosity. The parameter η'' has no special name but is related to the storage modulus through $G' = \eta''\omega$.

There are two different types of methods to determine linear viscoelastic behavior, *static test* and *dynamic test*. The static tests involve of a step change in strain or stress, and then an observation in time of the strain or stress. The dynamic tests involve the application of a harmonically varying strain [3].

When rheological tests are performed, it is important that the sample is homogeneous. If the sample is a dispersion or a suspension, it is important that the ingredients are very small with respect to the thickness of the liquid layer sheared, i.e. they have to be homogeneously distributed. This is because the sample must react to shear uniformly throughout. It is also important that the applied shear leads to a laminar flow. Much more energy is required to maintain turbulent flow than simply maintaining laminar flow. Thus the measured torque is no longer proportional to the true viscosity of a sample. Allowing turbulent flow in viscosity measurements would introduce big errors [1].

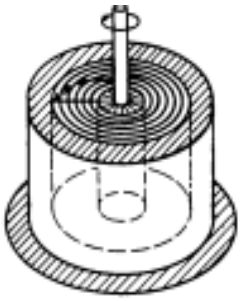

Figure 3.4: *A sketch of the rotor and the cylinder to a rheometer. Figure adapted from [1].*

3.3 Linear Elastic Fracture Mechanics

A material can be considered a linear elastic material when nonlinear and dissipative processes only concern a very limited volume of material around the crack tip, called the Fracture Process Zone (FPZ).

To develop a theoretical model of a dynamic crack growth process, the motion of the crack edge should follow from a mathematical statement of a *crack growth criterion*. Such a criterion must be related to some physical parameter defined as a function of the crack edge mechanical fields. Such a physical quantity is given by the dynamic energy release rate $\mathcal{G}$. $\mathcal{G}$ is the total mechanical energy release rate, and is determined by the mechanical fields near the crack surface [24].

In the study of crack growth process, the most commonly used crack growth criteria is the generalization of the Griffith critical energy release rate criterion. According to the generalized Griffith criterion, the crack must grow in such a way that $\mathcal{G}$ is always equal or bigger to Γ. Γ denotes the *fracture energy*, the energy needed to create a crack of unit length [24].

A crack in an ideally elastic solid stays stable if the amount of mechanical energy $\mathcal{G}$ per unit area released by the solid as the crack propagates by an infinitesimal length, does not overcome the energy per unit area dissipated to create two new fracture surfaces. Then the Griffith criterion for crack propagation reads [25]:

$$\mathcal{G} \geq \Gamma \tag{3.21}$$

The crack starts to move once the Griffith's criterion is fulfilled and $\mathcal{G} = \Gamma$. Under quasi-static conditions, the crack velocity is proportional to the difference between the static energy release rate $\mathcal{G}$ and Γ [25]:

$$\frac{1}{\mu} v = \mathcal{G} - \Gamma \tag{3.22}$$

where μ is the effective mobility of the crack front, v is the crack velocity and $\mathcal{G}$ is the amount of energy per unit area present at the tip of a static crack. When v becomes important, the quasi-static assumption stops being valid and the energy balance at the crack tip is predicted to have the form [26]:

$$\Gamma = \mathcal{G}(l) A(v) \approx \mathcal{G}(l) \left(1 - \frac{v}{c_R}\right) \tag{3.23}$$

Here l is the instantaneous crack length, A(v) is a universal function of v and c_R is the Rayleigh wave speed, i.e. the velocity of acoustic waves propagating along the surface of the considered material. $\mathcal{G}(l)$ is the amount of energy per unit area present at the tip of a static crack of length l and contains all of the effects of the applied stresses and specimen geometry. The equation can be inverted to give the expression for the motion for a dynamically moving crack [26]:

$$v(l) = c_R \left(1 - \frac{\Gamma}{\mathcal{G}(l)}\right) \tag{3.24}$$

This equation is valid as long as crack growth is slow enough. As $\mathcal{G}(l)$ can be arbitrarily large, equation 3.24 predicts that v can be arbitrarily close to its limiting velocity, c_R.

Theory tells us that if a crack propagates and maintains its motion in a forward direction, the crack will eventually reach a constant velocity equal to the Rayleigh speed c_R. That is because elastic energy given to the solid by the fracture must be transferred to the crack tip in order to break atomic bonds for crack extension, and this can only go as fast as the speed of sound on the cracks surface [27].

3.3.1 Straight cracks

Consider the case of a straight crack in a two-dimensional medium under tension as shown in figure 3.5. The stress field σ exhibits a square root singularity at the crack tip and is given as [25]:

$$\sigma_{ij} \approx \frac{K}{\sqrt{2\pi r}} F_{ij}(\theta) \tag{3.25}$$

Here r is the distance to the crack tip and θ is the angle with respect to the crack, the functional forms of $F_{ij}(\theta)$ are universal and K is called the *stress intensity factor* and depends on the crack length, on the specimen geometry and on the applied tension. $F_{ij}(\theta)$ is universal in the sense that it does not depend on the crack length or the detail of the applied loading. It depends on the angle with respect to the crack and on the properties of the material.

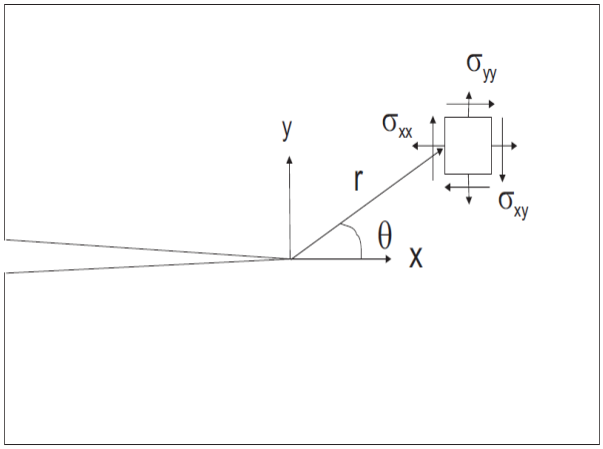

Figure 3.5: *Sketch and notation describing the stress field in the vicinity of a slit crack tip in a two-dimensional medium. Figure adapted from [25].*

It is convenient to distinguish between three different modes of crack propagation as shown in figure 3.6. Mode I, the tensile mode, corresponds to a crack propagating in a plane perpendicular to the uniaxial tensile stress. Mode I is the mode studied in the experiments performed in this thesis. Mode II, the shearing mode, corresponds to a shear of the crack walls in a direction normal to the crack front. Mode III, the tearing mode, corresponds

to a shear parallel with the crack front. Any set of loading conditions can be decomposed into a sum of these three basic modes [25].

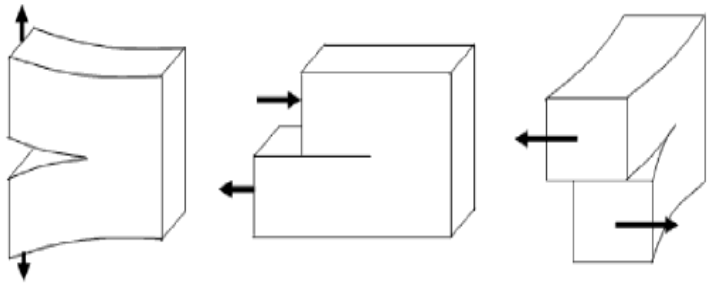

Figure 3.6: *The three modes of fracture: the tensile mode (mode I), shearing mode (mode II) and tearing mode (mode III). Figure adapted from [25].*

3.4 Fingering/fracturing in Hele-Shaw cells

The phenomenon of interfacial motion between two immiscible viscous media in the narrow gap between two parallel plates (a Hele-Shaw cell is seen in figure 3.7) is considered, and the phenomenon is nowadays known as the Saffman-Taylor instability [28, 7]. The motion in a Hele-Shaw cell is mathematically analogous to two-dimensional flow in a porous media [7]. In the experiments performed in this thesis, the two viscous media used are air (viscosity $\sim 1,82 \cdot 10^{-5}\text{Pa} \cdot \text{s}$ [29]) and clay suspension. When a less viscous medium (air) pushes a more viscous medium (clay suspension) a finger or a fracture appears, depending on whether the medium is fluid or solid.

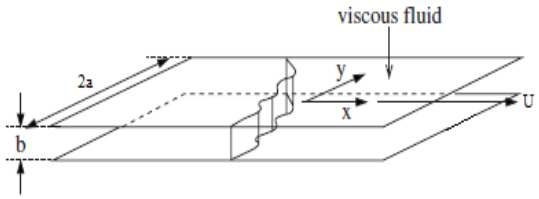

Figure 3.7: *Sketch of the Hele-Shaw cell geometry. Figure adapted from [30].*

If the pattern that appears in the Hele-Shaw cell is a "viscous finger" or a "viscoelastic fracture" (crack), depends on the medium in the Hele-Shaw cell. If the medium is a fluid, a viscous finger will appear, and if the medium is a solid, a fracture will appear [31, 29].

There are two variants of Hele-Shaw cells that are used in this thesis: *Linear* cells (channels) and *radial* cells. In channels, the less viscous fluid is pushed through one of the short sides of the cell while the other short side and the two long sides are closed. In radial cells, the less viscous fluid is injected through a hole at the center of the top plate while both of the long sides, and both of the short sides are closed [32].

3.4.1 Viscous fingering

Hydrodynamic instability was first discovered by Saffman and Taylor in 1958, and has served as a reference in the field of pattern formation [2]. Viscous fingering (VF) takes place at the interface between two fluids with different viscosities perlocating through a porous bed. When the fluid with the lower viscosity penetrates into the fluid with the higher viscosity, a planar boundary between the fluids is unstable against small perturbations, and a complex pattern resembling fingers can be seen [33].

Imagine an experiment where two circular glass plates are placed horizontally on top of each other, and separated by thin spacers. One of the plates has a central injecting hole. First the cell is filled with a viscous fluid, then air is blown into the central hole so as to push the oil out radially. Then one will have the pattern like the one shown in figure 3.8.

The slow flow of an incompressible fluid in a homogeneous porous medium is set by Darcy's law and the equation of continuity:

$$\vec{u} = -\frac{k}{\eta}\nabla p = \nabla\phi \tag{3.26}$$

$$\nabla \cdot \vec{u} = \nabla^2\phi = 0 \tag{3.27}$$

Here $\vec{u}$ is the velocity vector, p the pressure, k is the permeability of the medium and ϕ is the velocity potential. In rectangular configurations, e.g.

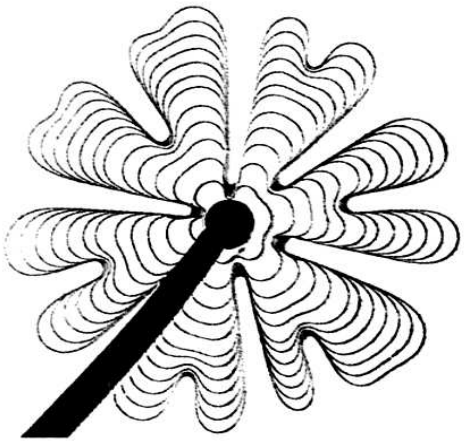

Figure 3.8: *A superposition of successive states of a radial Saffman-Taylor pattern. Figure adapted from [2].*

Hele-Shaw cells, the system evolves until a single finger (the Saffman-Taylor finger) forms. Here, the two-dimensional motion of an incompressible viscous fluid between two parallel plates is such that the components of the mean velocity satisfy [34, 35]:

$$\vec{u} = -\frac{b^2}{12\eta}\nabla p = \nabla\phi \tag{3.28}$$

In comparison with equation 3.26 and 3.27 it is shown that the motion in a Hele-Shaw cell is equivalent to two-dimentional flow in a porous medium of permeability $\frac{b^2}{12}$ where b denotes the gap of the cell [34, 35].

We adopt the notation from Mc Lean and Saffman [34] that U is the velocity of the finger, $2a$ is the lateral width of the Hele-Shaw cell, and b is the gap thickness ($\frac{b}{a} << 1$) as illustrated in figure 3.7. T is the interfacial tension between the driven (outside finger) and driving fluids, and η is the viscosity of the driven fluid. The parameter λ will denote the ratio of the width of the finger to the width of the Hele-shaw cell $\lambda =$*(width of finger)/(Width of cell).* The surface tension effects are neglected at the free surface, then experiments [7] yield that $\lambda = \frac{1}{2}$. As surface tension effects become important, the finger widens to fill the cell, and the agreement becomes poor. As the speed of the finger is increased the width steadily approach the limiting value of one half

of the channel width, and for very slow rates of advance, almost all the cell contents are swept out [34, 36]. When $\lambda \to 0$ the anisotropic finger does not feel the walls any more, and its growth becomes free [37].

3.4.2 Viscoelastic fracturing

Viscoelastic fluids are characterized by at least one internal relaxation time t_r, which characterizes the time scale of the structural reorganizations within the fluid. If the time scale of a flow event, t_{fl}, is much shorter than t_r, the medium responds as an elastic body. In the opposite case, it behaves as a liquid. This can be rationalized by introducing the *Deborah number* [18]:

$$D_e = \frac{t_r}{t_{fl}} \tag{3.29}$$

For $D_e << 1$, the viscous effects dominate and the system behaves as a fluid. For $D_e >> 1$, the elastic effects dominate and the system behaves essentially as an elastic solid. By decreasing the D_e, one can think of a possible crossover from fractal growth by flow to fractal growth by fractures. The crossover occurs for a critical value of D_e. There have been made attempts to determine this value in earlier studies [31].

When a viscoelastic fluid with a $D_e > 1$ is broken open by injecting a less viscous media, viscoelastic fractures (VEF) will appear. VEF is a structural instability which is driven by the release of elastic stress.

An idealized fracture is shown in figure 3.9. It is assumed that the material outside the failure zone in figure 3.9 is linearly viscoelastic, and the material within the zone to be highly nonlinear and viscoelastic. $y = 0$ corresponds to the plane of the fracture, and the y-axis is embedded in the continuum. The crack-tip is a straight line or curve in space, whose intersection with the x-y plane is defined by the point $P(x = \mathrm{a}, y = 0)$. In the failure zone, there exist some significant attractive interatomic forces. In practise, the boundary between the undamaged continuum and the material in the failure zone is rather diffuse, but it is assumed that it exists a boundary as seen in figure 3.9. The *apparent* crack-tip is defined to be at $x = \mathrm{a}_b$, and often in literature, the apparent crack-tip is used as the crack-tip [38].

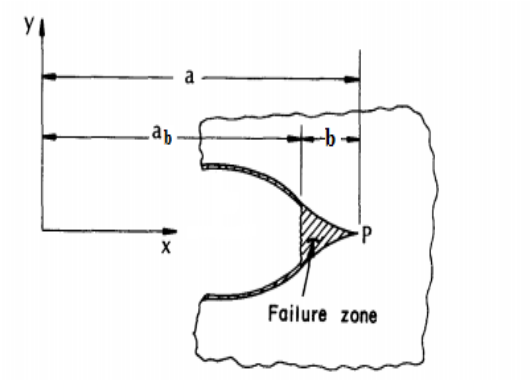

Figure 3.9: *Cross-section of an idealized fracture. Figure adapted from [38].*

3.5 Sol-gel transition

Though all liquids exhibit viscoelastic structure, we consider a sol (or solution) a fluid with no apparent elastic behavior and a gel as a material exhibiting an elastic response to external force. In rheological terms, a sol can be described as a fluid where the loss modulus G'' exceeds the storage modulus G' and the opposite for a gel. The sol-gel transition state will then be where $G'' \approx G'$. A gelling solution at the sol-gel transition is a unique state of matter that is neither liquid nor solid, but is in a transition between these states [39]. During gelation, polymers undergoe a phase transition from a sol to a gel. In the transition, the monomers go from not being connected in a sol, to being connected in a gel [40]. So the sol-gel transition is characterized by the divergence of viscosity in the sol, and by the appearance of an elastic behavior in the gel phase [41].

3.5.1 Perlocation theory

Perlocation describes the geometrical transition between disconnected and connected phases as the concentration of bonds in a lattice increases. Let p denote the concentration of polymers, so when p exceeds a critical value p_c, a cluster is formed which extends throughout the whole system. Under these conditions, the system changes from a finite distance scale to an infinite value; and this is the so called *perlocation threshold* or the *gel point*. The viscosity η and the elastic modulus can then be given as [42, 40]:

$$\eta \propto (p - p_c)^{-m} \tag{3.30}$$

$$G \propto (p - p_c)^{n} \tag{3.31}$$

The behavior of η and G in the close vicinity of the gel-point is illustrated in figure 3.10.

Another way to determine the gel-point is based on small deformation oscillatory flow measurements at a constant frequency. In the case of chemical gels a gel-point criterion is the equality condition $G' = G''$ [42]. In experiments, the complex shear modulus $G*$ is usually measured, with the result that *at the gel point* both the storage G' and loss G'' parts of the modulus are power laws in frequency,

$$G'(\omega) \sim G''(\omega) \sim \omega^{\Delta} \tag{3.32}$$

By a Fourier transform it can then be shown that the shear relaxation modulus, which describes the stress after a constant shear strain, must decay as $G(t) \sim t^{-\Delta}$ where Δ is the *viscoelastic exponent* [43]. The gelation time can be determined from the crossover of the elastic G' and viscous G'' moduli. It follows from equation 3.32 that the ratio G''/G' at the gelling time can be expressed as [44]:

$$\left[\frac{G''(\omega)}{G'(\omega)}\right]_{t=t_g} = \tan(\Delta\pi/2) \tag{3.33}$$

The gelling time is thus defined as the time at which the ratio G''/G' is independent of frequency. Equation 3.33 is the most generally valid gel point criterion [40].

In prior studies, Martin and Wilcoxon [39] used the technique of quasielastic light scattering to probe the dynamics of the sol-gel transition. With the help of this technique, the scattered intensity $I(q,t)$ can be found. Regardless of the form, all known $I(q,t)$ can be described by a characteristic time τ. Martin and Wilcoxon have demonstrated that in a gelling solution the characteristic time τ diverges at the sol-gel transition.

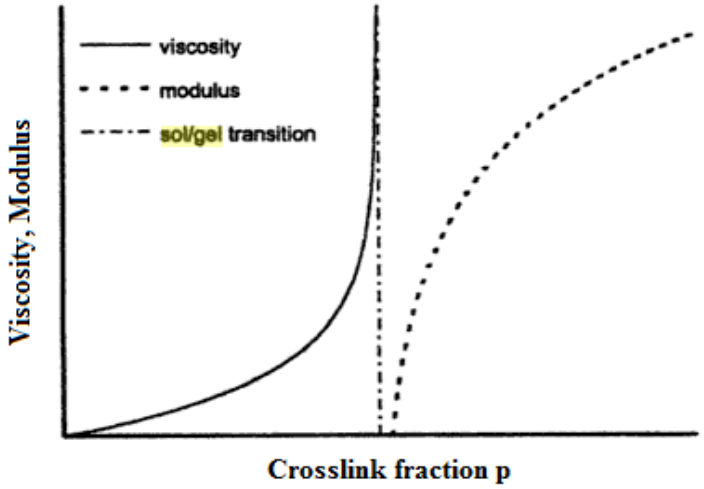

Figure 3.10: *Behavior of the viscosity and the elastic modulus in the close vicinity of the sol-gel transition. Figure adapted from [42].*

3.6 Liquid crystals

Liquids are always isotropic. Compared to crystals, they do not have a preferred orientation and are not orientation dependent. This is due to thermal motion not having an orientation preference. There is a special class of molecules, which inhibit an inner ordering that spontaneously develops in the liquid phase such that a macroscopic anisotropy arises. These kind of molecules are rod-like particles, called *nematogens*, and the anisotropic state is called the *nematic state*. Compared to the isotropic distribution, there is an orientation distribution with a well-defined preferred overall orientation [47]. While the nematic phase shows a rotational ordering, it exists an other state, called the *smectic* phase that inhibits both rotational and positional ordering as shown in figure 3.11. Each state has unique mechanical, optical, electrical and chemical properties [49].

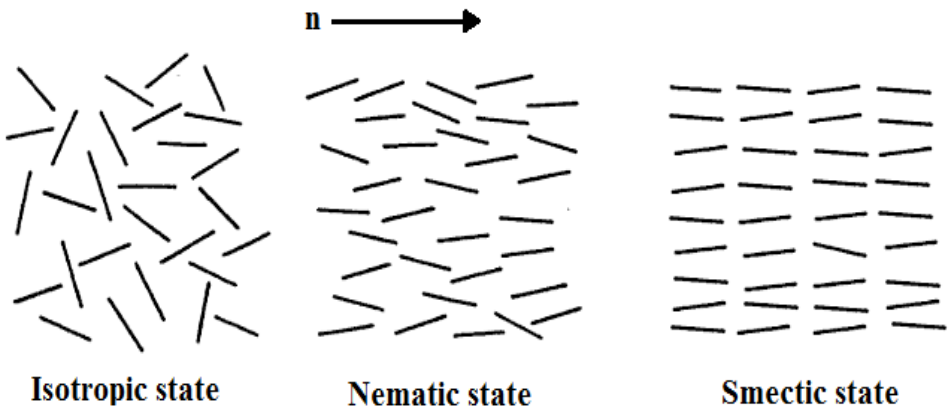

Figure 3.11: *The microscopic structure of the isotropic, nematic and smectic state for rod-like molecules. Figure adapted from [48].*

3.6.1 The Nematic state

The sketch in the middle of figure 3.11 shows the microscopic structure of the nematic state. The centers of gravity of the rod-like molecules are arranged as in a liquid, but the difference from the isotropic state is that there is no isotropic distribution of the orientation of the molecular axes. There is an orientation distribution, but with a well-defined preferred overall orientation. The preferred direction is not constant over the whole sample, but it changes slowly over the macroscopic (μm) length-scales. The preferred direction is characterized by a unit vector, the *nematic director*, denoted by $\mathbf{n}$. This is illustrated in figure 3.11. The physical meaning of $\mathbf{n}$ is the direction of the optical axis [47]. The nematic director has the property $\mathbf{n} = -\mathbf{n}$, the sign is of no importance as the operation of turning the system 180 degrees still will conserve all the physical properties of the nematic. The nematic director $\mathbf{n}$ can be seen in the figure 3.12 as the direction of the red arrows. $\mathbf{n}$ gives the average orientation of the nematogens within a volume of the nematic phase [52].

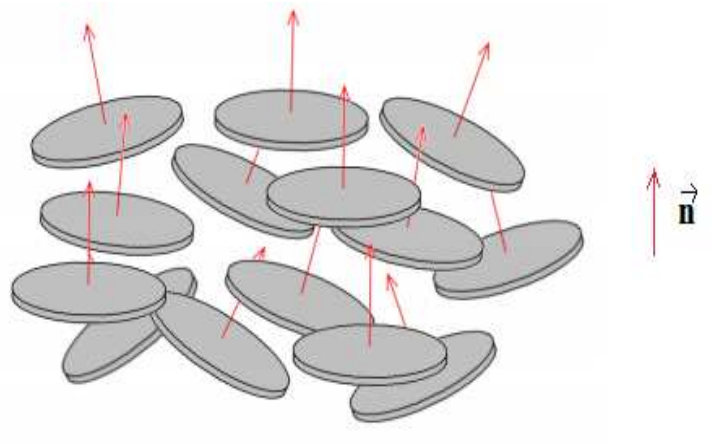

Figure 3.12: *The orientational order of a nematic, of disc-like colloids. The average direction of the red arrows gives the nematic director. Figure adapted from [52].*

The degree of orientational ordering is represented by the *order parameter,* S_2, which is defined by:

$$S_2 = \frac{1}{2} < 3\cos^2\theta - 1 > \tag{3.34}$$

Where θ is the angle between the long axis of an individual molecule and the nematic director, and "<>" denotes an ensemble average. S_2 approaches 1 for perfect ordered molecules, and zero for isotropics [49].

Laponite clay suspension is in the nematic state above a certain concentration as shown in figure 3.13. The concentration that gives the nematic state can be depicted from figure 3.13, and is found to be 3 wt%.

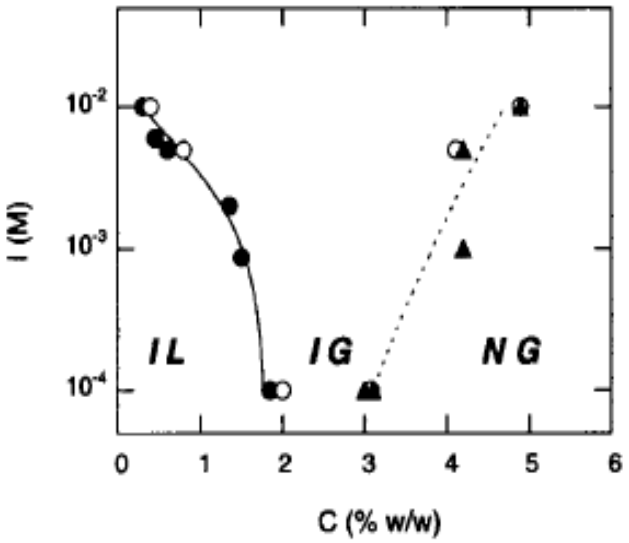

Figure 3.13: *The phase diagram for Laponite clay suspension, showing at which concentration the nematic state occur. IL denotes Isotropic Liquid, IG denotes Isotropic Gel and NG denotes Nematic Gel. Data points are obtained by rheological (filled circles), osmometric (open circles), and birefringence (filled triangles) data. I(M) denotes the Ionic strength, and C(% w/w) denotes the concentration. Figure adapted from [50].*

3.7 Polarization

Polarization is a characteristic of all transverse waves. For a string that lies along the x-axis, the displacement may be along the y-axis as illustrated in figure 3.14. Then the string lies in the x-y plane. When a wave only moves along the y-axis, the wave is said to be linearly polarized in the y-direction. For mechanical waves, *polarizers* can be build, that only let waves with a certain polarization through. In figure 3.15, the string can slide freely in the y-direction, but no motion in the z-direction is possible [51].

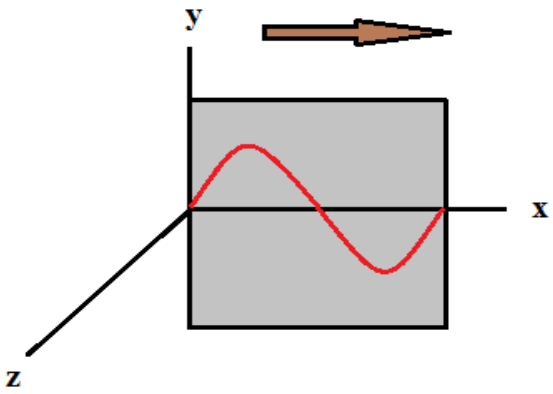

Figure 3.14: *Transverse wave on a string polarized in the y-direction. Figure adapted from [51].*

All of this can be applied to electromagnetic waves, which also have polarization. An electromagnetic wave is a *transverse* wave, as the example with the string above. An electromagnetic wave consists of both electric and magnetic fields, which are perpendicular to each other and to the propagation direction. The polarization of an electromagnetic wave is always defined as the direction of the electric-field vector, $\vec{\mathbf{E}}$. An electromagnetic wave polarized in the y-direction can be written as [51]:

$$\vec{E}(x,t) = E_{max}\cos(kx - wt)\hat{y} \tag{3.35}$$

$$\vec{B}(x,t) = B_{max}\cos(kx - wt)\hat{z} \tag{3.36}$$

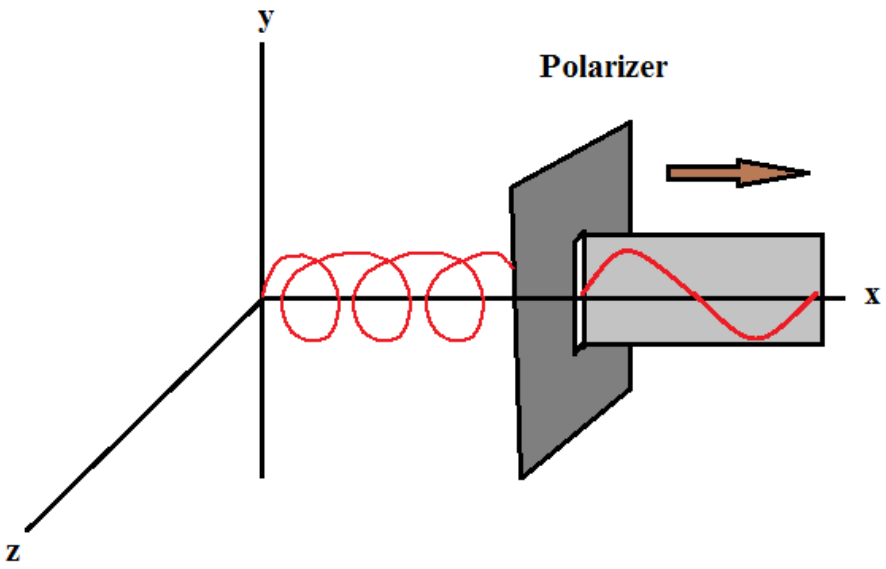

Figure 3.15: *A polarizing filter, that only passes components polarized in the y-direction, but blocks those polarized in the z-direction. Figure adapted from [51].*

3.7.1 Polarizers

Light from ordinary light sources, such as light bulbs and sunlight, is *always* unpolarized. To create polarized light from unpolarized light, a polarizer as in the figures 3.15 and 3.16 is needed. An ideal polarizer, produces linear polarized light from unpolarized light, and passes 100% of the incident light that is polarized in the direction of the filter's polarizing axis but completely blocks out the light that is polarized perpendicular to the axis [51].

Crossed polarizers are two polarizers with their transmission axis perpendicular to each other. Then the light with any polarization will not pass through. It is possible that the light can pass the first polarizer, but it will be blocked by the second one. If an optical element that changes the state of polarization of the light is placed between the two crossed polarizers, the light whose polarization has been change will be transmitted [46].

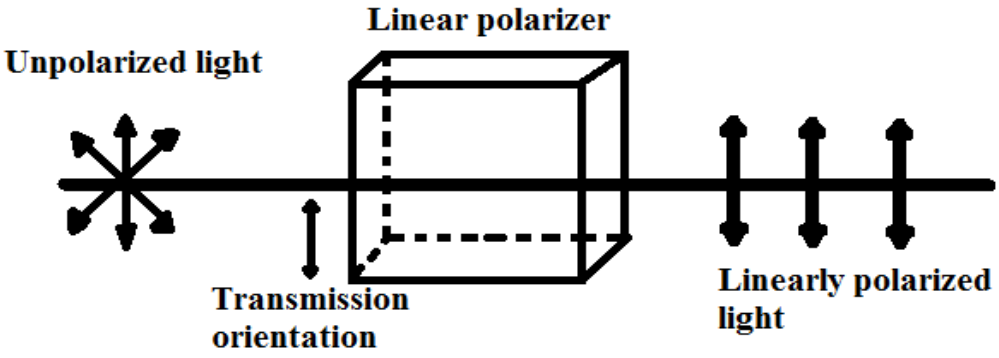

Figure 3.16: *The basic principle of a linear polarizer. Unpolarized light enters the polarizer and linear polarized light is transmitted.*

Birefringence

An electromagnetic wave in vacuum propagates with a speed $c = 1/\sqrt{\epsilon_0\mu_0}$, but a wave propagating through a material medium travels at a speed $v = 1/\sqrt{\epsilon\mu}$. Here ϵ and μ denotes the permittivity and permeability of the medium. The *index of refraction*, n, is then defined by [54]:

$$n \equiv \frac{c}{v} = \sqrt{\frac{\epsilon\mu}{\epsilon_0\mu_0}} \tag{3.37}$$

An optically isotropic material has a index of refraction that is the same in all directions. This is obtained for cubic crystals as well as for noncrystalline substances. However, in anisotropic materials, the binding forces on the electron clouds are different in different direction and therefore the refractive indices are as well. A material that exhibits *birefringence*, has difference indices of refraction for different directions of polarization. So, when two waves with equal amplitude and perpendicular directions of polarization enter such materials, they travel with different speeds. The material alters the phases of the two waves. This means that birefringent materials can convert linearly polarized light into circularly polarized light, and circularly into linearly polarized light. *Uniaxial birefringent* crystals encompass the trigonal, hexagonal and tetragonal systems, and they contain a single symmetry axis known as the optic axis. They then display *two* distinct indices of refraction. The birefringence magnitude is then defined by [51, 54]:

$$\Delta n = n_c - n_o \tag{3.38}$$

Where n_o and n_e are the refractive indices for polarization perpendicular (ordinary) and parallel (extraordinary) to the axis of anisotropy respectively.

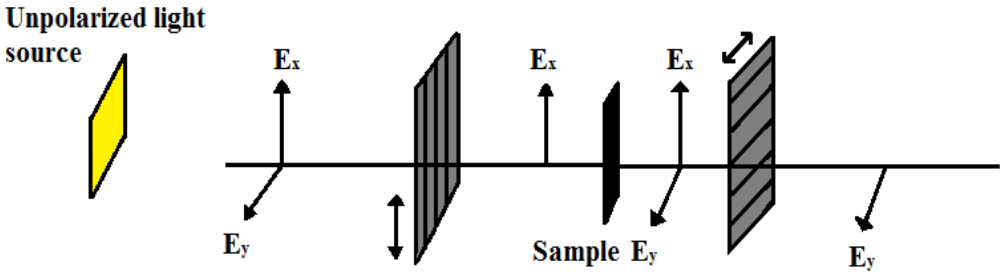

Figure 3.17: *Example of a setup used when observing birefringence from a liquid crystalline sample. Figure adapted from [53].*

Figure 3.17 gives an example of a setup used to observe birefringence in a sample. An unpolarized source is followed by a polarizer and an analyzer, with a sample of liquid crystalline (or any other anisotropic material) between them. Unpolarized light enters the polarizer, the light gets polarized, and only light polarized along the x-axis gets transmitted. Then the light enters the sample, get altered, and the light is then polarized along both the x- and the y-axis. At last, the light enters the analyzer, and only light polarized along the y-axis is transmitted. If the sample had not been between the polarizer and the analyzer, or if the sample did not exhibit birefringence, the light had not been altered, and there had not been any light transmitted after the analyzer.

Chapter 4

Experimental

4.1 Preparation of samples

4.1.1 Laponite gel

A clay known as Laponite RD in powder form is purchased from Laporte Ltd. The suspension used in these experiments consists of 3 wt% or 3,5 wt % Laponite RD and 97 wt% or 96,5 wt% distilled water. The Laponite powder is added to the distilled water while the water is being stirred. The clay suspension is prepared under room temperature $\sim 23^{\circ}$ Celsius, and stirred for around 1 hour to make sure all the Laponite is uniformly dissolved in the water. The Laponite clay suspension has a constant temperature of $\sim 23^{\circ}$ Celsius. The sol-gel transition state can then be found by rheometry. More information about Laponite can be read in the section 2.1.1.

4.1.2 Bentonite

The clay suspension of Bentonite is prepared by mixing Bentonite powder, which is purchased from Damolin FUR, and distilled water under room temperature $\sim 23^{\circ}$ Celsius. The Bentonite powder was crushed using a mortar made of marble, since the particles are so large, such that it is difficult to make them dissolve completely in the water for high concentrations of Bentonite. The suspension is stirred for 24-48 hours to make sure all the Bentonite powder is uniformly dissolved, while being enclosed to prevent evaporation of water from the sample. The Bentonite clay suspension need to be stirred for a longer time than the Laponite clay suspension, since the particles in

the Bentonite powder are larger than the particles in the Laponite powder. Samples with different concentrations were made to find which concentrations suited the best to perform experiments in the Hele-Shaw cells. There were made samples with concentrations ranging from 5 up to 12 wt% Bentonite. The samples with 11 wt% and 12 wt% Bentonite were too viscous to be used. They solidified while stirring, and are not fitted to be used for the kind of experiments that are performed in this thesis. The samples with 5, 6 and 7 wt% bentonite were too liquid to be used. They had almost the same viscosity as water, and will then use a too large amount of time to get viscous enough to perform experiments with.

In the experiments performed in this thesis, samples with concentrations of 8, 9 and 10 wt% Bentonite were used. More information about Bentonite can be read in the section 2.1.2.

4.2 Rheological measurements

To know when the Laponite clay suspension solidifies, the Physica MCR300 Rheometer from Anton Paar, shown in figure 4.1, is used to find the sol-gel transition state of the suspension. An amount of 17 ml of Laponite clay suspension is injected in the cylinder, seen in figure 4.1b, before a rotor is lowered into the cylinder.

(a) *An overview of the rheometer.*

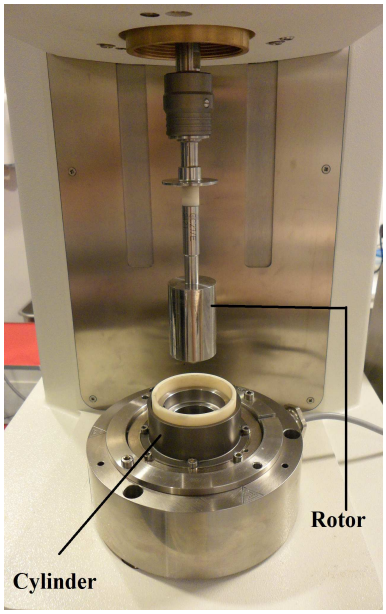

(b) *Zoom in of the rheometer, showing the rotor and the cylinder.*

Figure 4.1: *The Physica MCR300 Rheometer.*

An oscillatory frequency test was performed on the Laponite clay suspension with the rheometer for ten up to twelve hours. The experiments were performed with a strain $\gamma = 2\%$, frequency $\omega = 10$ s^{-1}, temperature $T = 23°$ Celsius.

There were not performed tests with the Bentonite clay suspension in the rheometer. This is because the Bentonite clay suspension is not homoge-

neous[1]. The Bentonite particles are too large compared to the thickness of the liquid layer sheared, so they are not completely homogeneously distributed. Because of this, the sample does not react to shear uniformly throughout.

4.3 Experiments with the Hele-Shaw cell

4.3.1 Setup I

Setup I is a linear Hele-Shaw cell. As seen in figure 4.2 the cell consists of two rectangular plates made of Plexiglas separated by two retractable plates (pistons), which are made of metal, placed on the two long sides of the cell. The pistons are covered with velvet, causing good adhesion with the clay suspension. The pistons can be pulled apart causing a finger/fracture to appear in the sample, which is in the channel between the pistons. Two motors are connected to the two pistons with metal rods, causing the pistons to be pulled apart parallel and steady. The motors are connected to a computer that controls the motors using the program *WinPos*. To see the complete settings on WinPos, see appendix B.

The cell lies on top of a wooden plate, that has a rectangular hole such that a light table can be placed below, as seen in figure 4.2a. The light table is needed such that it is possible to record the fingering/fracturing with a camera from above as seen in figure 4.2b. In this setup fracturing/fingering will be studied during the liquid state, the sol-gel transition state and the gel state to clay suspensions. The channel inside the cell is 50 cm long, the height is 3 mm, and the width starts at 3.5 cm and can be pulled until 8.5 cm.

For experiments in the liquid state there are used samples with a concentration of 3 wt% Laponite, and for the sol-gel transition state there are used both samples with 3 wt% and with 3,5 wt% Laponite. For experiments in the gel state there are used samples with a concentration of 3,5 wt% Laponite. It is used a higher concentration of Laponite during the experiments in the gel state than in the liquid state. This is because the sample needs to be a

[1] To perform a rheological test, the sample must be homogeneous as discussed in section 3.2

gel to achieve fractures, and the higher the concentration, the faster the clay suspension solidifies. It can not be used higher concentrations than 3,5 wt% Laponite, because for higher concentrations the sample will solidify while stirring.

The clay suspension is injected through one of the short sides of the Hele-Shaw cell as seen in figure 4.2a, which is left open, while the other short side is closed. Before the suspension is injected, some grease is added with a syringe in the closed end before the top plate is attached to prevent air leakage. Then the suspension is injected with a syringe while the cell is a little tilted and the top plate is attached to prevent the suspension to flow out of the cell again. It is very important to avoid air bubbles in the sample when the suspension is injected, since each of these bubbles will intervene with the finger/fracture and become a singularity. The finger will wrap around the bubble, and then looses its shape and direction. The fracture intends to propagate towards the bubble. After the suspension is injected in the channel, the air bubbles can be removed using a long wire with a little angle in one of the ends. The wire is inserted inside the open end with the little angle first to "pull" out the bubbles. The clay suspension is left in the cell for a desired amount of time, while the open end is covered to prevent evaporation of water from the sample. The motors are started using the program WinPos on the computer. The pistons are pulled apart with a velocity of 1, 5, 10, 20 or 30 mm/s during the liquid state, and with a velocity of 1, 5 and 10 mm/s during the sol-gel transition state and with a velocity of 1 and 5 mm/s during the gel state. The fingers/fractures that appear in the channel when the pistons are pulled apart are recorded using a PROSILICA GX camera located above the cell, as seen in figure 4.2b. The camera is connected to the computer and is controlled using the software LabVIEW[2]. To see the complete labVIEW and camera settings, see appendix A. It is important that the cell is completely horizontal to keep the finger/fracture propagating straight forward. To do this, a level can be placed upon the cell to see if the cell is leveled, and then build it up until it is leveled.

[2]A software to control mechanical devises, such as cameras

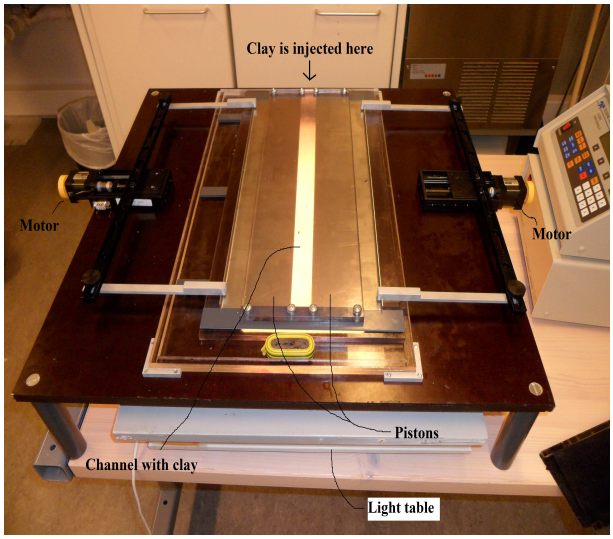

(a) *An overview of setup I.*

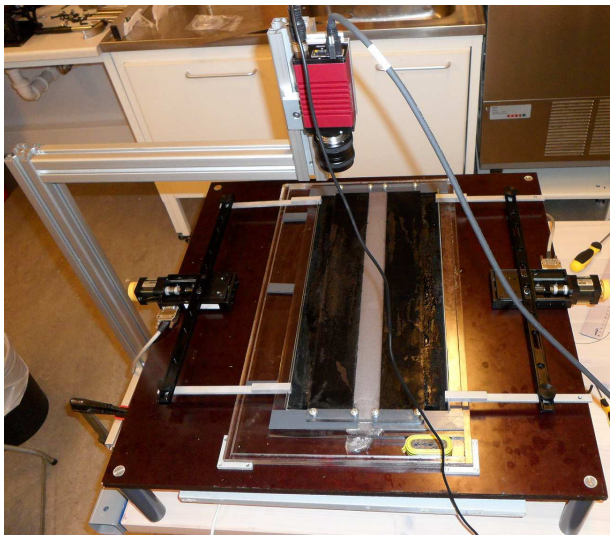

(b) *Setup I with the camera connected and velvet on the pistons.*

Figure 4.2: *Setup I.*

Setup I with crossed polarizers

There is one polarizer, polarizer 1, that is placed on top of the light table between the light table and the wooden plate as seen in figure 4.3. The other polarizer, polarizer 2, is placed on top of the cell and has its transmission axis 90 degrees to the transmission axis to polarizer 1. The experiments are performed in the same way as in setup I, the only difference is that the cell lies between the two crossed polarizers. Around polarizer 1, black paper/fabric is placed since polarizer 1 does not cover the whole light table. This is important, because unpolarized light must be hindered to enter the cell, and polarizer 2. There are performed experiments in the liquid state, at the sol-gel transition state and in the gel state of Laponite clay suspension.

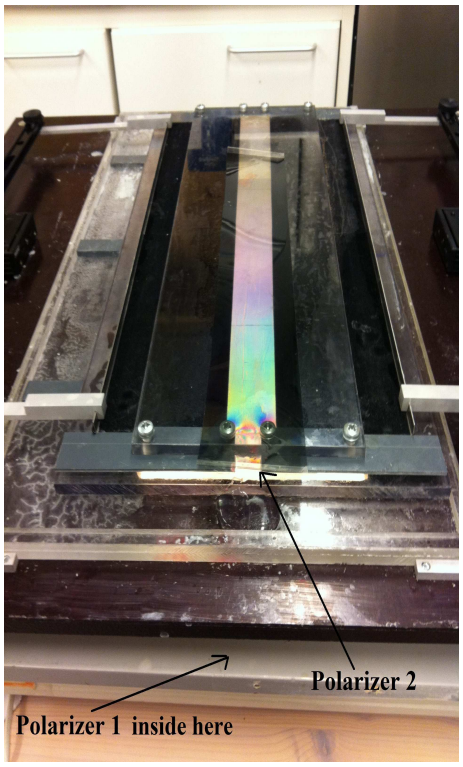

(a) *A picture of setup I with crossed polarizers.*

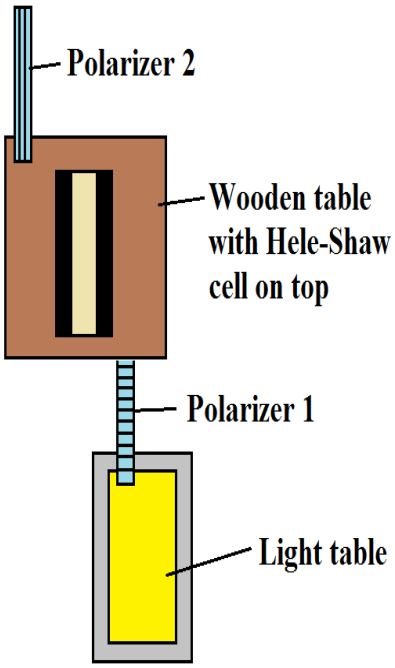

(b) *An illustration of setup I with crossed polarizers*

Figure 4.3: *Setup I with crossed polarizers.*

4.3.2 Setup II

Setup II is similar to setup I, but is a radial Hele-Shaw cell instead of a linear cell and can be seen in figure 4.4. The clay suspension is injected in the channel before the top plate is attached. This is because it is not possible to inject the suspension through the hole in the middle when the top plate is attached. The channel is then 3,5 cm wide and , and there is a lot of air in the channel. If the clay suspension is to be injected, the suppressed air will have nowhere to go, and it will be impossible for the suspension to flow into the cell. After the sample is spread evenly throughout the channel, the top plate is attached. It is important to prevent air bubbles, and to prevent an air layer between the sample and the top plate, because this will ruin the fractures/fingers. An air layer between the sample and the top plate will cause the finger/fracture to propagate up into the layer. In the end, the hole in the middle of the cell must be covered to prevent evaporation of water from the sample. The sample is left in the cell for different amounts of time, depending on what kind of study is desired.

As seen in figure 4.4, the cell is closed in both ends, so the finger/fracture propagates from the hole in the middle of the cell. The hole has a diameter of 2 cm, the channel is 50 cm long and has a height of 3 mm. When the experiment is ready to be done, the motors get started, the pistons are pulled apart, and the fingers/fractures get recorded using a PROSILICA GX camera located above the cell.

The clay suspensions are left in the cell for an amount of time ranging from 1 hour up to 72 hours, and consist of concentrations of 8, 9 and 10 wt% Bentonite.

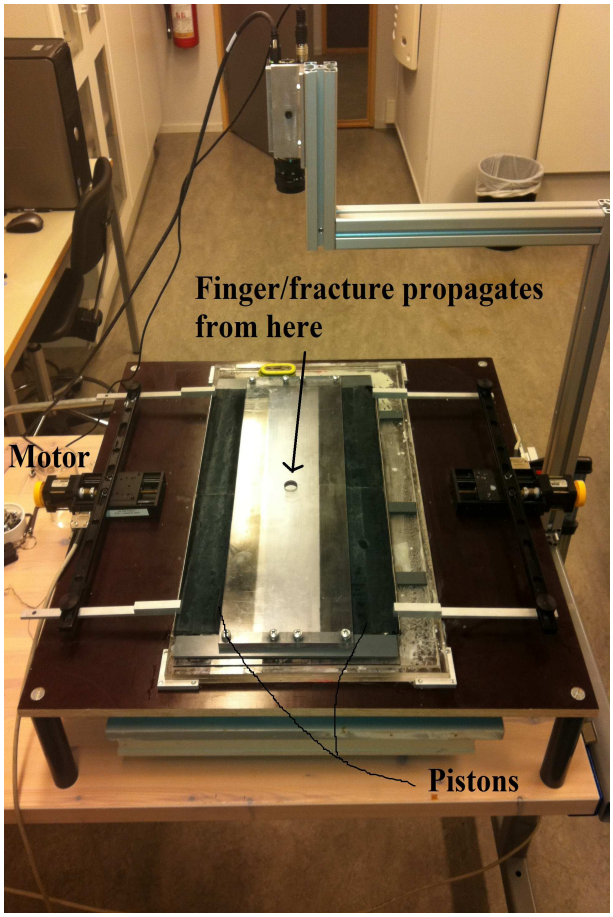

Figure 4.4: *Setup II.*

Chapter 5

Results and discussion

5.1 Rheological measurements

The results from the rheometer are shown in figure 5.1. From these graphs, the sol-gel transition state to Laponite clay suspensions with concentrations of 3 wt% and 3,5 wt% can be extracted. If fracturing/fingering is to be studied near the sol-gel transition state, the clay suspension has to be in the cell for the amount of time extracted from the graphs, before the experiments can be performed. The sol-gel transition state is found where the storage modulus, G' crosses the loss modulus, G'' in figure 5.1. In figure 5.1a, it can be extracted that the sol-gel transition state for 3 wt% Laponite clay suspension occurs after about 5000 seconds ($\sim$ 1,4 hours). For 3,5 wt% Laponite clay suspension the sol-gel transition state occurs after about 500 seconds ($\sim$ 8,3 minutes) as seen in figure 5.1b. So the higher the concentration of Laponite is, the less amount of time before the sol-gel transition state occurs.

It is possible that these values depend on the amount of sample that is in contact with air, small concentration differences in the suspensions, and the temperature of the room the tests are performed in. This leads to some time differences for the sol-gel transition state in the rheometer and in the Hele-Shaw cell. In the rheometer, the samples are in greater contact with air than in the Hele-Shaw cell, such that the time before the transition state occurs is longer in the cell than in the rheometer. Because of this, the results from the rheometer cannot be transferred and used in the experiments in the Hele-Shaw cell.

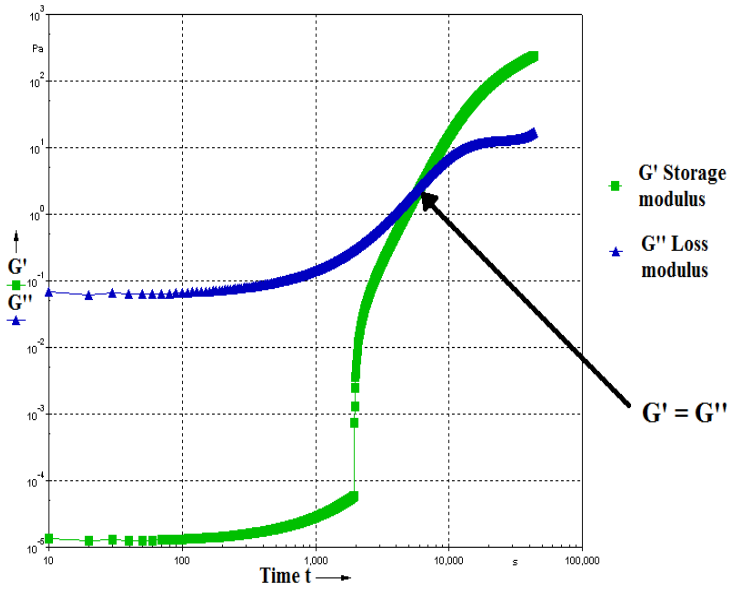

(a) *Rheological test for 10 hours with a clay suspension consisting of 3 wt% Laponite.*

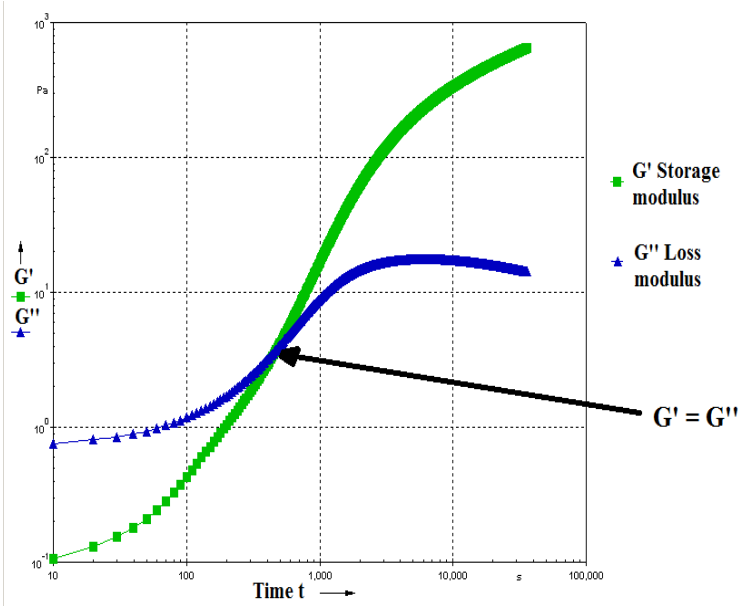

(b) *Rheological test for 10 hours with a clay suspension consisting of 3,5 wt% Laponite.*

Figure 5.1: *Rheological tests with different concentrations of Laponite, showing the storage and loss modulus as a function of time.*

5.2 Setup I

The cell is sealed, such that an air layer between the suspension and the top plate is prevented, and there is minimal evaporation of the suspension. Problems with this setup were that it appeared some contamination from the velvet that covers the pistons. This contamination could blend with the clay suspension, and may have interfered its rheological behavior. The cell was not completely leveled, this could be due to the plates in the cell not being of uniform thickness, or that the wooden plate could be uneven due to the weight of the cell upon it, or due to the properties of the wood. When the cell is unleveled, it can interfere with the finger/fracture propagating in the sample. Especially the finger intended to propagate more to one side, than the other. It was also difficult to make the cell completely air proof, causing some air leakage in the closed end and through the pistons. To prevent this, grease was added in the closed end of the cell. The problem with air leakage was a greater problem during the gel state, than during the liquid state, since then the suspension had been for a longer amount of time in the cell and the probability for evaporation and air leakage was greater.

Experiments were done both before, during and after the clay suspension had solidified. Before the clay suspension had solidified, the loss modulus G' was greater than the storage modulus G'', fingering was studied, as shown in the figures in 5.2 and 5.3. After the clay suspension had solidified, G'' was greater than G', fracturing was studied, as shown in the figures in 5.8. While $G' = G''$, the sol-gel transition state was studied as shown in the figures in 5.5 and in 5.6. Sometimes the fingers/fractures penetrated unevenly in the clay suspension. This could be caused by impurities in the suspension or by tiny air bubbles which are almost impossible to avoid. In many fracturing experiments, some branches in the fractures can be observed. In the fracturing experiments, the tensile mode (mode 1) can be seen as described in section 3.3.1. There was a difference between the fingering and the fracturing. During fingering, the tip was more curved and penetrated more uniformly than during fracturing. During fracturing, the crack tip was sharper, and it penetrated more arbitrary, often with an angle of 90 degrees to the penetration direction.

The liquid state

Experiments were performed in the liquid state using different velocities of the pistons. The experiments were performed with the velocities 1, 5, 10, 20 and 30 mm/s. An experiment was performed with the velocity 50 mm/s as well, but the motors were not strong enough to pull the pistons apart using this velocity, so the motors just stopped. The experiments performed in this state achieved good results.

The width of the finger should depend on the velocity of the pistons. According to the theory discussed in section 3.4.1, the width of the finger should be narrower for greater velocities. As can be seen in figure 5.2, this is not the case in these experiments. This can be a result of the surface tensions being crucial in this cell. The age of the clay had a large influence on the width of the finger. The older the clay was, the narrower the finger width became. This can be seen if the fingers in figure 5.3 are compared to the fingers in figure 5.2. In figure 5.3, the clay suspension had been in the cell for 5 hours, and the fingers were significantly narrower than the fingers in figure 5.2, where the clay suspension had been in the cell for 1,5 hours.

However, mostly the finger penetrated evenly in the clay suspension, and air leakage was avoided in the liquid state. The sample used in these experiments consisted of a concentration of 3 wt% Laponite.

There are some differences in the finger widths to the fingers in figure 5.3. This can be due to the clay suspension not being exact 5 hours old for each experiments. It can also be due to small concentration differences in the laponite clay suspension. This is more crucial when the clay suspension starts to solidify, than when the suspension is a liquid. The finger width decreased with ~ 30 % when the age of the clay suspension went from being 1 hour to 5 hours old. This was found by comparing the width of the finger compared to the width of the channel for the experiments with 1 hour and 5 hours old clay suspension using the experiment with the velocity 10 mm/s. This is illustrated in figure 5.4. If the clay suspension stays in the cell for an even longer time, the fingers become more and more narrow, until they turn into fractures.

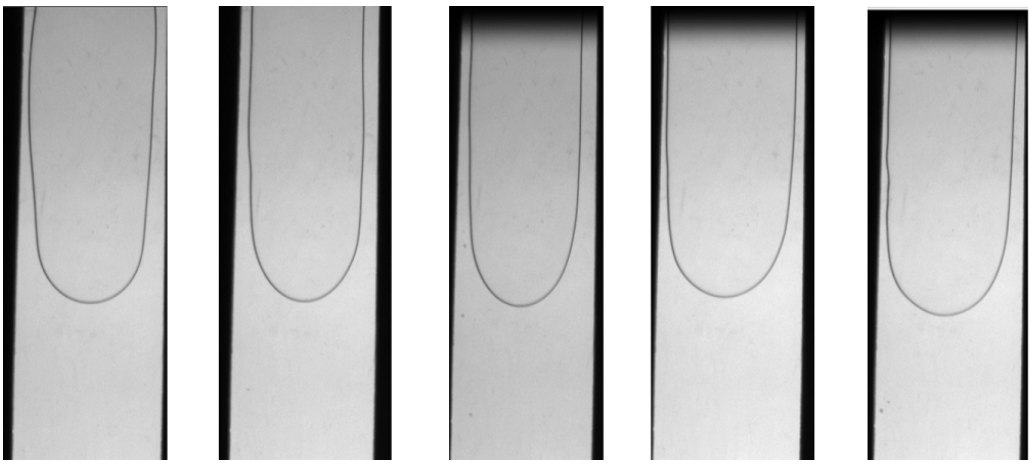

Figure 5.2: *Finger-experiments performed after the clay suspension had been in the cell for 1 hour, and the pistons were pulled with a velocity of 1, 5, 10, 20 and 30* mm/s *respectively from left to right. The Laponite clay suspension consisted of 3 wt% Laponite.*

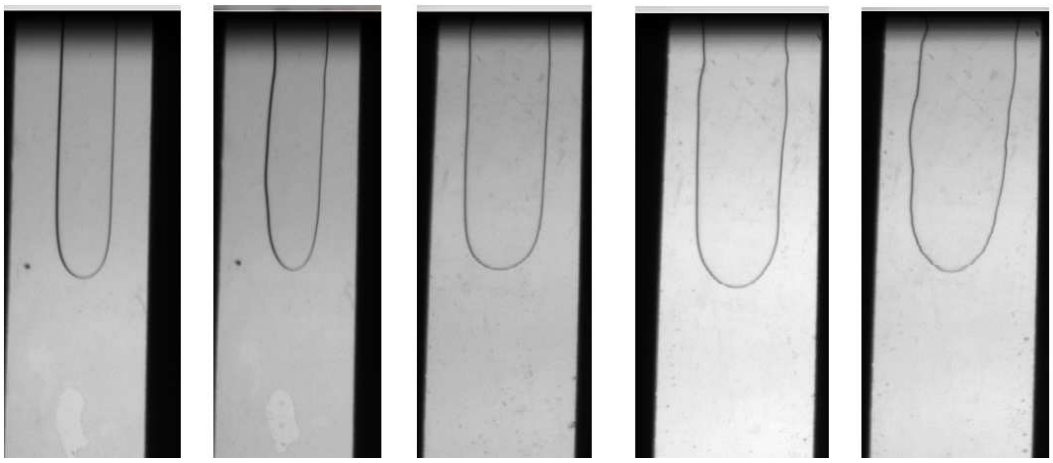

Figure 5.3: *Finger experiments performed after the clay suspension has been in the cell for 5 hours, and the pistons were pulled with a velocity of 1, 5, 10, 20 and 30* mm/s *respectively from left to right. The Laponite clay suspension consisted of 3 wt% Laponite.*

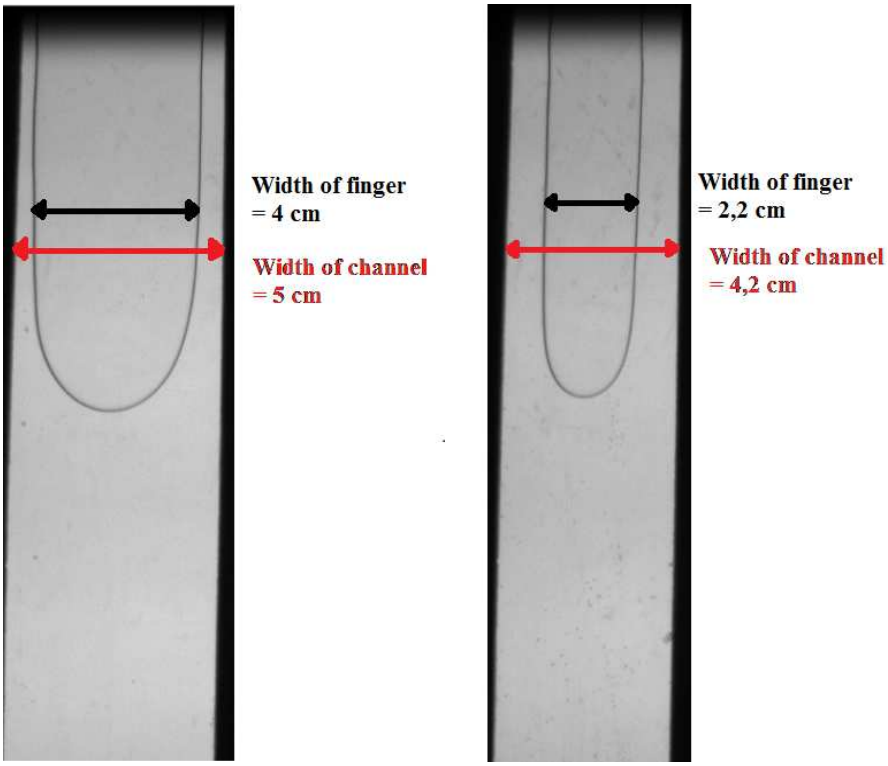

Figure 5.4: *A comparison of the finger width compared to the channel width between 1 hour old and 5 hours old clay suspension using the velocity 10* mm/s. *The finger to the left was performed after 1 hour, and the finger to the right was performed after 5 hours. The Laponite clay suspension consisted of 3 wt% Laponite.*

The sol-gel transition state

The rheometer was used to find the sol-gel transition state, but the conditions in the rheometer were different from the conditions in the Hele-Shaw cells. This made the results from the rheometer render useless, so the amount of time before the sol-gel transition state occurred could not be found accurately. By doing experiments it could be extracted that the amount of time before the transition state occurred for a suspension of 3,5 wt% Laponite was around 1 day.

It was done experiments using clay suspensions with both 3 wt% Laponite, and with 3,5 wt% Laponite. These two suspensions have a different gelling time. This can be seen in if the figures in 5.5 and the figures in 5.6 are compared. In figure 5.5, it was used a clay suspension with 3 wt% Laponite. These formations are more finger-like than the formations in figure 5.6. In figure 5.6 it is used a clay suspension with 3,5 wt% Laponite. The clay has started to solidify more, and the formations are more fracture-like. In figure 5.5 the formations are like thin fingers, the finger tips are almost curved, and they penetrate evenly throughout the clay suspension. It can be assumed that the sol-gel transition state has not yet occurred. In figure 5.6 the formations are more like a mix of a finger and a fracture. The tips are still a little curved, but the fingers/fractures do not penetrate evenly in the clay suspension, and some branches can be seen. It can be assumed that the suspension is under the sol-gel transition state.

In the experiments performed with the clay suspension with 3 wt% Laponite, the formations did not change much with the different velocities. There is minimal changes in the finger width which can be due to some small time differences in the different experiments. In the experiments performed with the clay suspension with 3,5 wt% Laponite, the formations did not change much either. It seems that the age of the clay is much more significant than the speed of the pistons.

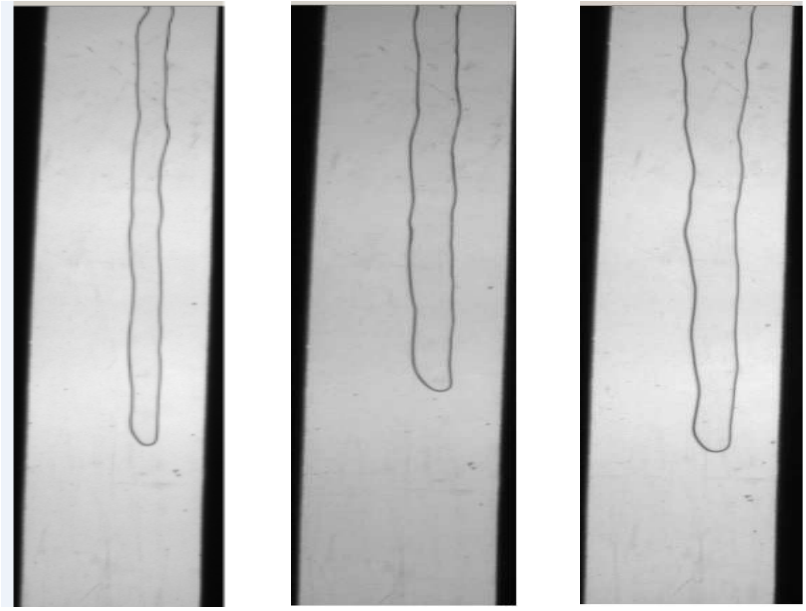

(a) *Finger/fracture made when the pistons were pulled with a velocity of 1* mm/s.

(b) *Finger/fracture made when the pistons were pulled with a velocity of 5* mm/s.

(c) *Finger/fracture made when the pistons were pulled with a velocity of 10* mm/s.

Figure 5.5: *Fingering/fracturing made after the clay suspension had been in the cell for 25 hours, and the clay suspension consisted of 3 wt% Laponite.*

The gel state

In the gel state, experiments were also performed with different velocities of the pistons. The velocities used were 1 and 5 mm/s. To achieve the gel state, the Laponite clay suspension stayed in the cell for 2 and 3 days. There were only performed experiments at two velocities in the gel state, since these experiments did not give good results. The biggest problem with the experiments in this state was that air leakage appeared after a while. This resulted in air bubbles in the sample after a day or two, or air entering through the closed end. As mentioned above, this ruins the fracture. An example of this can be seen in figure 5.7. In this figure it can be observed air leakage from the closed end and from the pistons.

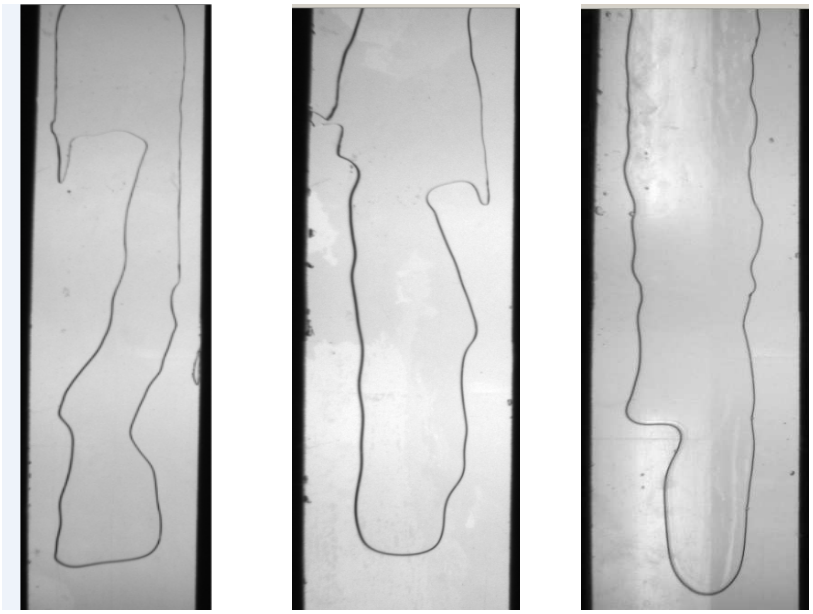

(a) *Finger/fracture made when the pistons were pulled with a velocity of 1* mm/s.

(b) *Finger/fracture made when the pistons were pulled with a velocity of 5* mm/s.

(c) *Finger/fracture made when the pistons were pulled with a velocity of 10* mm/s.

Figure 5.6: *Fingering/fracturing made after the clay suspension had been in the cell for 25 hours, and the clay suspension consisted of 3,5 wt% Laponite.*

A thin syringe was used to suck out the smallest air bubbles, but the larger bubbles were more difficult to remove. This caused the results from the fracture experiments being not so good. The experiments performed after 1 day went better than the experiments performed after 2 and 3 days, since after 1 day the air leakage was less significant than after 2 and 3 days. The problem was that after 1 day, the clay suspension is not as solid as after 3 days. The sample used in these experiments consisted of a concentration of 3,5 wt% Laponite. There were performed experiments after 2 days and after 3 days using the velocities 1 and 5 mm/s. The experiments performed after 2 and 3 days can be seen in figure 5.8.

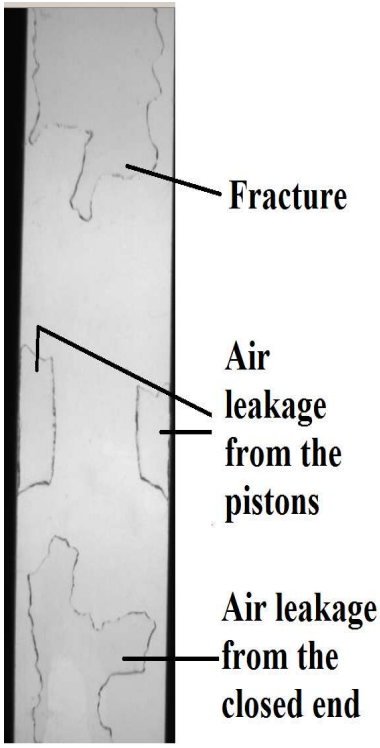

Figure 5.7: *An example of a fracture experiment where air leakage have appeared. The clay suspension has been in the cell for 45 hours and the pistons are pulled apart with the velocity 1* mm/s

As seen in the figure 5.8, the crack tips are sharper and penetrate more arbitrary than in the liquid state. In the fractures, branches out from the ordinary tip can be seen. These branches do not appear in the liquid state. There are not so many differences from the sol-gel transition state, but it can be seen that the crack tips are sharper in the gel state. To see if there are differences in the fractures for different velocities, more experiments need to be done with several velocities. This could not be done here, since most of the experiments gave bad results due to the problems with air leakage.

The fractures did not change much from the fractures made after 2 days, to the fractures made after 3 days. After 2 days, the clay suspension has become a gel, and it does not solidify much more during 1 more day. This can

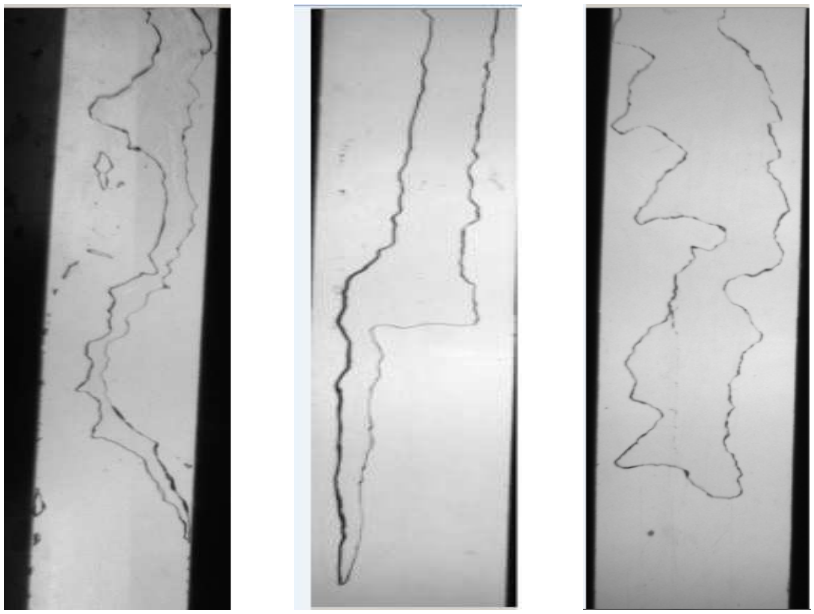

(a) *Fracture made when the pistons were pulled with a velocity of 1* mm/s*, and the clay suspension has been in the cell for 48 hours.*

(b) *Fracture made when the pistons were pulled with a velocity of 5* mm/s*, and the clay suspension has been in the cell for 48 hours.*

(c) *Fracture made when the pistons were pulled with a velocity of 10* mm/s*, and the clay suspension has been in the cell for 72 hours.*

Figure 5.8: *Fracturing in 3,5 wt% Laponite clay suspensions after the suspension has been in the cell for 48 and 72 hours.*

be studied further for older clay suspensions if an air proof Hele-Shaw cell is made. It can be interesting to study fracturing for Laponite clay suspensions several days older than 3 days, when the suspension has become even more solid-like.

5.2.1 Setup I with crossed polarizers

There were performed experiments using setup I with crossed polarizers. Light was let through the two polarizers when no clay suspension was present in the cell, since the plates are made of Plexiglas. Plexiglas is weakly birefringent, such that the polarization of the light gets altered. This can be seen in figure 5.9. The different colors are due to some bending of the plates that affects the wavelengths, and hence the different colors.

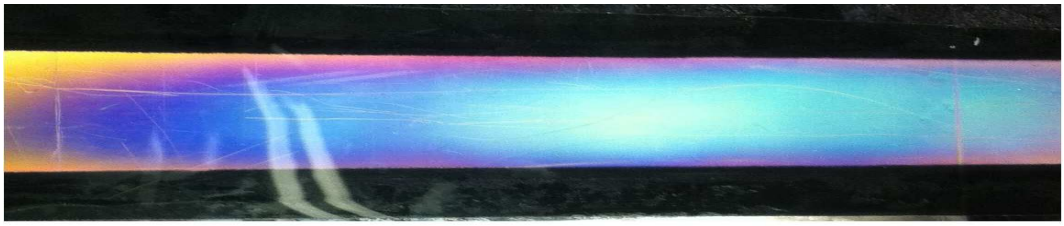

Figure 5.9: *An empty cell between crossed polarizers.*

There were no alterations of the light when the clay suspension was present in the cell as seen in figure 5.10. Here the suspension had been in the cell for 68 hours, and consisted of 3,5 wt% Laponite. The colors are a little different from the colors in figure 5.9, which is an empty cell. This can be due to the two Plexiglas plates being screwed more loosely or tightly together. It can also be due to which angle the picture is taken from. There were no changes in the colors during a time span of 70 hours.

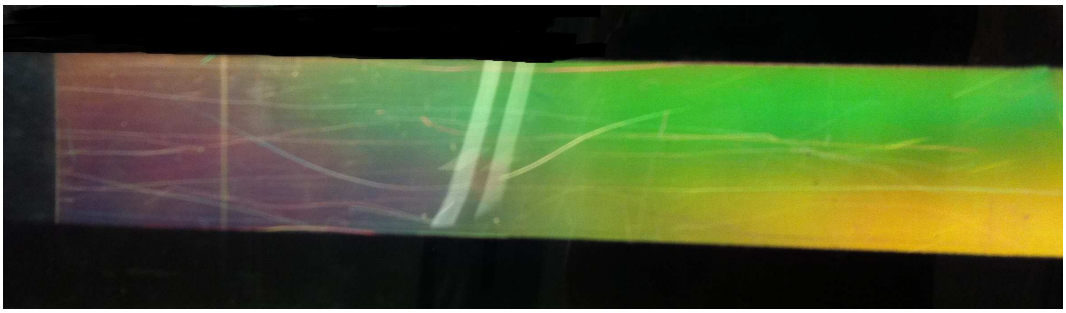

Figure 5.10: *Clay suspension that has been in the cell for 68 hours, and which has not yet been performed experiments on. The cell is placed between crossed polarizers.*

Experiments with crossed polarizers were first performed in the liquid state to the Laponite clay suspension. There was no difference in the finger experiments with crossed polarizers from the experiments without crossed polarizers. This can be due to the extension of the nematic ordering is smaller in the liquid state, than in the gel state. This makes it more difficult to see the ordering in the liquid state. This is shown in figure 5.11. The colors in this picture are due to some bending in the plates.

Figure 5.11: *Finger made after the clay suspension has been in the cell for 1 hour, and the pistons were pulled with a velocity of 5* mm/s*. The experiment is performed using crossed polarizers and a clay suspension of 3,5 wt% Laponite.*

Experiments were also performed after 1-3 days. In these experiments ordering at the crack tip and in the clay suspension in the cell could be seen, as shown in figure 5.12. The experiments were performed after the clay had been in the cell for 1, 2 and 3 days respectively. The differences were not so great from the experiment performed after 1 day compared to the experiment performed after 3 days. The clay suspension was more solid-like after 3 days than after 1 day such that the formation was more fracture-like, but the ordering was nearly the same during the three days. During an experiment the nematic ordering is relocated around the crack tips, making the nematic ordering easier to see.

After the experiment was performed, the pistons were pushed together again, the starting point was achieved, and the clay suspension was whole again. The interesting factor is that the nematic ordering in the suspension could be seen as shown in figure 5.13. It can be seen that in the top picture there is some ordering that cannot be seen in the bottom picture. The nematic

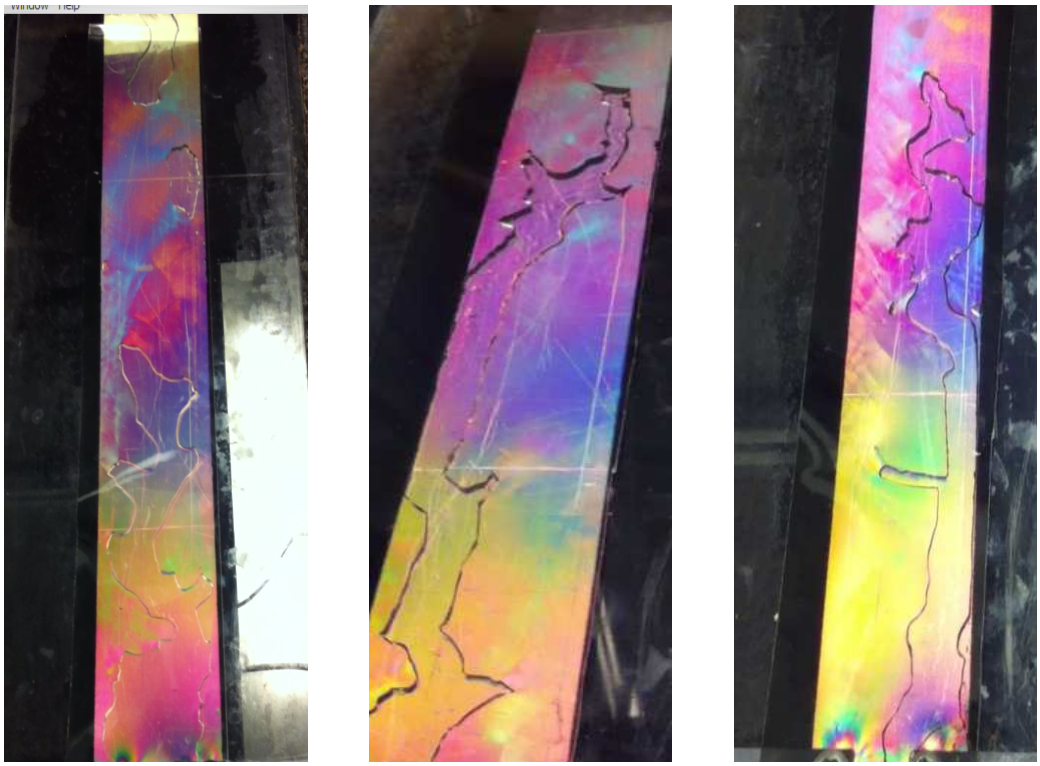

(a) *Fracture made after the clay suspension had been in the cell for 25 hours.*

(b) *Fracture made after the clay suspension had been in the cell for 43 hours.*

(c) *Fracture made after the clay suspension had been in the cell for 68 hours.*

Figure 5.12: *Fracture experiments performed using crossed polarizers and the pistons were pulled with a velocity of 1* mm/s*. The experiments were performed using a clay suspension of 3,5 wt% Laponite.*

ordering seen in the the top picture, can both be due to the nematic ordering that was relocated during the experiments and due to adhesion between the clay suspension and the Plexiglas plates.

In the pictures in figure 5.14, a zoom in of the fractures made using crossed polarizers can be seen. In these pictures, a better view of the nematic ordering is shown. From these pictures, it can be extracted that there are not much differences in the ordering during the three days.

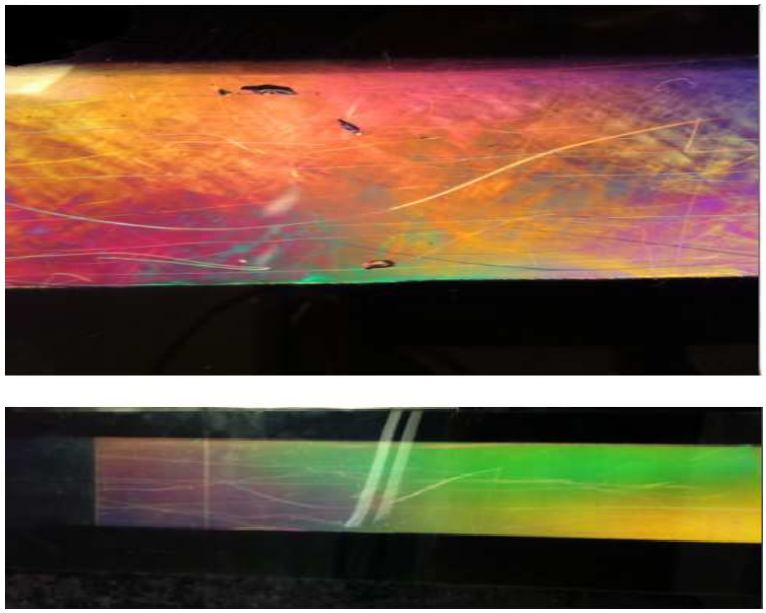

Figure 5.13: *The top picture shows the suspension after it had been in the cell for 70 hours, and the pistons have been pushed together again after an experiment. The sample is a clay suspension with 3,5 wt% Laponite. The bottom picture shows the clay suspension before an experiment was performed. The suspension had been in the cell for 68 hours, and the suspension was the same as in the top picture.*

(a) *A zoom in of the fracture made after the clay suspension had been in the cell for 25 hours.*

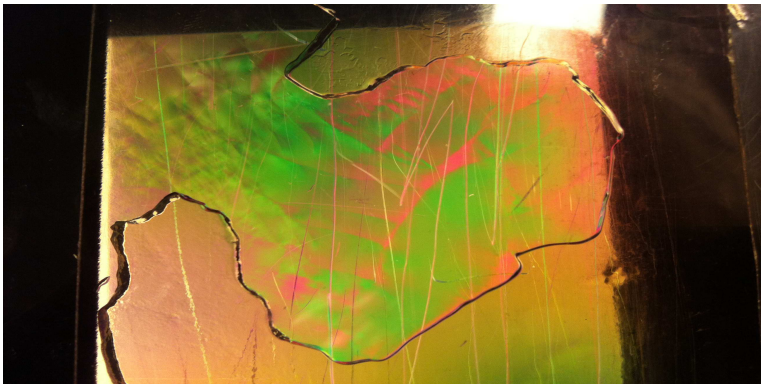

(b) *A zoom in of the fracture made after the clay suspension had been in the cell for 43 hours.*

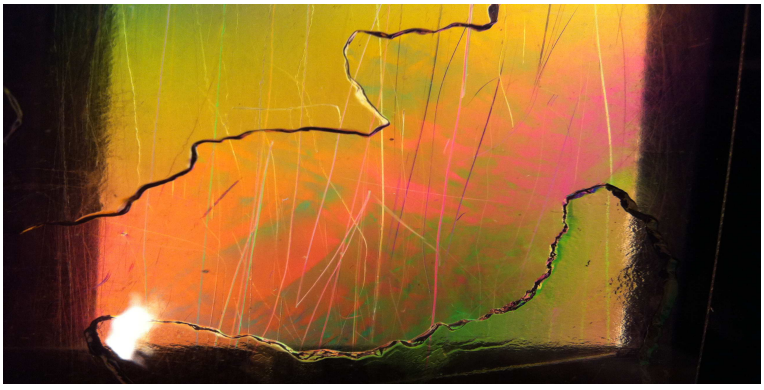

(c) *A zoom in of the fracture made after the clay suspension had been in the cell for 68 hours.*

Figure 5.14: *A zoom in of the fracture experiments performed using crossed polarizers and the pistons were pulled with a velocity of 1* mm/s*. The experiments were performed using a clay suspension of 3,5 wt% Laponite.*

5.3 Setup II

There were done different experiments with clay suspensions using different concentrations of Bentonite, and with different amount of time the sample was left in the Hele-Shaw cell. The concentrations ranged from 8 wt% up to 10 wt% Bentonite. The amount of time the sample was left in the cell ranged from 1 to 3 days, and the pistons were pulled apart using a velocity of 2 mm/s.

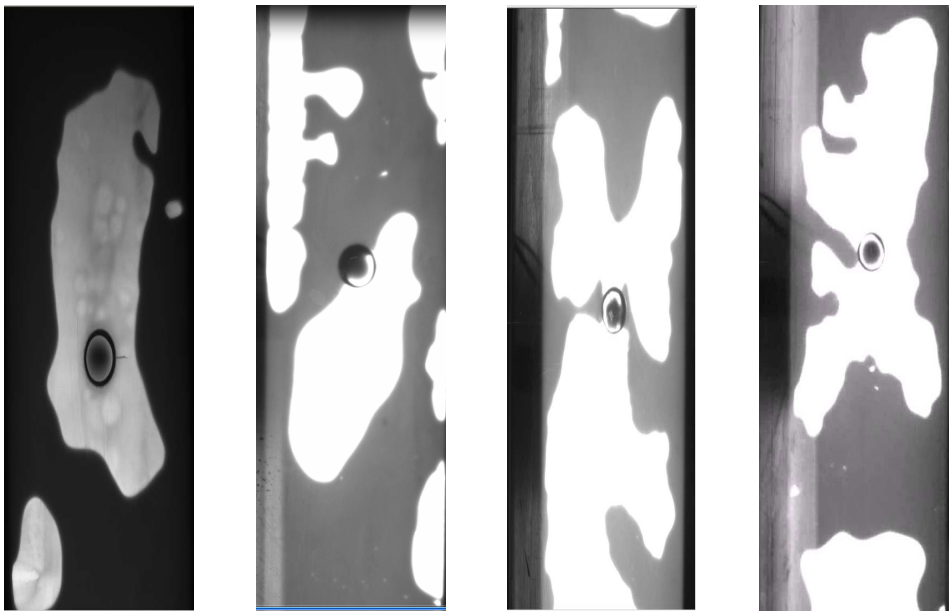

(a) *Experiment using a clay suspension with 8 wt% Bentonite after 2 days in the cell.*

(b) *Experiment using a clay suspension with 10 wt% Bentonite after 1 day in the cell.*

(c) *Experiment using a clay suspension with 9 wt% Bentonite after 3 days in the cell.*

(d) *Experiment using a clay suspension with 10 wt% Bentonite after 3 days in the cell.*

Figure 5.15: *Experiments using Bentonite clay suspensions with different concentrations of Bentonite, and with different ages of the clay suspension. The experiments were performed in a radial Hele-Shaw cell and the pistons were pulled apart using the velocity 2* mm/s.

The results were not that good. As can be seen in figures 5.15a, 5.15c and 5.15d, there was some air leakage in the channel. This can be seen as fingers/fractures other places than around the hole in the middle. This is because the cell was not completely sealed, so air could leak in through the ends, and through the pistons. In a radial Hele-Shaw cell it is important that the cell is completely sealed. If the cell is sealed, the pistons do not have to be covered by velvet, since there will be adhesion between the pistons and the sample if there is vacuum in the channel. The air bubbles are not that important either, since they will not lead to new fingers/fractures.

The gap between the top and the bottom plate, the height of the channel, was too large. This could lead to instabilities at the tip of the finger/fracture in three dimensions. This is not desirable, and complicates the finger/fracture. It is also possible that the finger/fracture propagates up between the sample and the top plate, since this is easier than to break through the bulk material. It will be better if the gap is 2-1 mm, instead of 3 mm.

There were some difficulties with injecting the sample into the cell. If the sample was injected through the hole in the middle, there was air in the channel that prevented the sample to spread throughout the channel. This was because the air that was already in the channel before the sample was injected had nowhere to go, and would make it impossible to inject the sample. If the sample was inserted in the channel before the top plate was attached to the cell, there was a risk that some air was left in the channel when the top plate was attached. The best way to inject the sample will be if one starts with the pistons pushed completely together. A cable can connect a syringe filled with sample to the hole in the middle of the top plate. Then, when the pistons are pulled apart the under-pressure will pull the sample out of the syringe, through the cable, and into the channel of the cell. It is important that the cable completely fills the hole in the top plate, such that an under-pressure will appear. This was done in the experiments performed by Baudouin Saintyves, explained in the section 6.2.

It will be easier to perform the experiments if the size of the hole in the top plate is smaller than r=1 cm. The hole does not need to be larger than r=5 mm. In the setup by Baudouin Saintyves seen in section 6.2, the hole had a radius of r=5 mm, and that gave good results. It will be easier to find a cable

that completely fills the hole, and it is also possible that the size can interfere with the finger/fracture, since the finger/fracture starts to propagate from the hole in the center of the top plate.

The experiments will be better if it is possible to change the symmetry of the cell. If this is possible, then the pistons do not have to be the long sides, but can also be the short sides. It will also be easier to perform experiments if the dimensions of the cell are smaller, and there is less volume in the channel.

Since these problems were too great to be dealt with in the amount of time I had, we had to go back to setup one. This was a setup that worked, and we would not have had the time to make a new radial cell that would have avoided all the problems mentioned above. To see what could have been done if I have had the time, see section 6.2.

Chapter 6

Conclusion and future studies

6.1 Conclusion

Experiments were done in both a linear and a radial Hele-Shaw cell. Experiments were first performed in setup I (the linear Hele-Shaw cell), and the experiments gave good results. Since these experiments worked well, experiments with setup II (the radial Hele-Shaw cell) were started. In setup II experiments were performed with Bentonite clay suspension consisting of 8, 9 or 10 wt% Bentonite. The clay suspension was left in the cell for an amount of time ranging from 1 hour up to 72 hours, and the pistons were pulled apart with the velocity 2 mm/s. After performing some experiments in setup II, it was discovered that it was not possible to do good experiments with this setup. This was because the setup was not completely air proof, so there appeared a lot of air leakage that ruined the experiments. We then went back to doing experiments with setup I, since this was a setup that worked and gave good results.

6.1.1 Setup I

In setup I, experiments were performed with Laponite clay suspension that consisted of 3 wt% or 3,5 wt% Laponite. The suspension with 3 wt% Laponite was used for the experiments in the liquid state and the sol-gel transition state, the suspension with 3,5 wt% Laponite was used for the experiments in the sol-gel transition state and in the gel state since this suspension solidifies faster than the one with 3 wt% Laponite. Experiments were performed with different aging of the clay suspension, and with different velocities of

the pistons. Experiments in the liquid state were performed when the clay suspension was from 1 to 5 hours old[1]and with the concentration of 3 wt% Laponite, while the experiments in the sol-gel transition state were performed when the suspension was 1 day old and with the concentrations 3 wt% and 3,5 wt% Laponite. Experiments in the gel state were performed when the suspension was 2 and 3 days old[2] and with the concentration of 3,5 wt% Laponite. In the liquid state, the sol-gel transitions state, and in the gel state, there were used different velocities of the pistons. There were performed experiments with the velocities 1, 5, 10, 20 and 30 mm/s in the liquid state, with the velocities 1, 5 and 10 mm/s at the sol-gel transition state, and 1 and 5 mm/s in the gel state.

In the liquid state the width and direction of the finger did not change with increasing velocities, as would have been expected from the theory. This could be due to the surface tensions being crucial. The finger width did decrease with increasing age of the clay suspension. During 5 hours, the finger width decreased with $\sim 30\%$. After 5 hours, a change in the finger width could be seen for the different velocities. This could both be due to some small changes in the concentrations or small changes in the age of the clay suspension. After around 1 day, it can be seen that the fingers gradually become fractures. For the suspension with a concentration of 3,5 wt% Laponite, the sol-gel transition state was found by experiments to occur after 24 hours. The formation was a mix of a finger and a fracture. The crack tip was more curved than in the fracture experiments, but the finger/fracture penetrated arbitrary in the clay suspension and some branches could be seen from the original tip. The fracture experiments were just performed with two velocities, since the fracture experiments did not give good results. Air leakage was a great problem during the gel state, because air leakage ruins the fractures. This was a greater problem during the gel state than the other phases, since in the gel state the clay suspension had stayed in the cell for the longest amount of time. In the fracture experiments the tips were sharp, and the fracture penetrated arbitrarily in the suspension. There also appeared branches out from the original tips. By these experiments it can be concluded that the shape of the finger depends much more of the concentration and age of the clay suspension, than of the velocity of the pistons.

[1]After 1 to 5 hours, the clay suspension is still in a liquid state.

[2]After 2 to 3 days, the clay suspension has started to solidify and becoming a gel.

6.1.2 Setup I with crossed polarizers

It was used crossed polarizers in setup I. The cell was placed in between two polarizers with their transmission axis perpendicular to each other. Experiments were performed when the clay suspension was 1 hour old to study fingering. This experiment did not give any different results from the experiment performed in the liquid state without crossed polarizers. This can be due to the extension of the nematic ordering being smaller in the liquid state than in the gel state, making the nematic ordering more difficult to see. There were also performed experiments when the clay suspension was 1, 2 and 3 days old. When the clay suspension had started to solidify, nematic ordering could be seen in the clay suspension showing the nematic state. There were not much difference in the nematic ordering after 1 day than after 3 days.

6.1.3 Rheological experiments

Rheological experiments were done using the Physica MCR300 Rheometer. There were done rheological experiments on the Laponite clay suspension with 3 wt% Laponite and on the Laponite clay suspension with the 3,5 wt% Laponite. For the 3 wt% Laponite suspension, the sol-gel transition state extracted from the rheometer was after 1,4 hours, while for the 3,5 wt% Laponite suspension it was after 8,3 minutes. This was not the case in the Hele-Shaw cell. In the Hele-Shaw cell the amount of time before the sol-gel transition state occurred, was longer than 1,4 hours or 8,3 minutes for the two suspensions. This could be due to the suspension being in greater contact with air in the rheometer than in the cell. The results from the rheometer could therefore not be used for the experiments in the Hele-Shaw cell.

6.2 Future studies

An idea for future studies is to copy the setup of Baudouin Saintyves as seen in figure 6.1. Sadly I did not have the time to make a copy of his setup during the time I had disposable after my stay at CEA in Paris.

To copy Baudouin's setup one will have to build a radial Hele-Shaw cell that is completely sealed and air proof, and where it is possible to change the symmetry. It should be possible to change the pistons to be either the long sides, or the short sides. To get the cell completely air proof, Baudouin did not have velvet on the pistons, but instead he had made tiny channels in the ends of the pistons, in these channels he had putted strips of rubber. He had two channels with rubber in each of the pistons, which can be seen in figure 6.1b. It should also be possible to change the size of the channel, depending on what kind of experiment is to be done.

It will be interesting to perform experiments with other materials as well as clay suspensions. Baudouin did a lot of experiments with micelles[3], which is a perfect Maxwell fluid[4]. It can be interesting to do experiments with different types of silicon oil, and also with other types of clay suspensions than the two suspensions used in this thesis.

If a completely air proof cell is built, it will be interesting to do experiments with Laponite clay suspensions at different velocities in the gel state. It will also be interesting to do experiments with clay suspensions several days older than 3 days, when the clay suspension has become more solid-like.

Experiments with Bentonite clay suspension can be performed in setup I as well as with setup II. It can be useful to study fingering and fracturing in the suspension, but studies with crossed polarizers cannot be done since the Bentonite clay suspension is non-transparent.

It will be interesting to do more studies of the Laponite clay suspension through crossed polarizers. It would be interesting to do studies with several

[3]Micelle is an aggregate of surfactant molecules dispersed in a liquid colloid. Micelles can be both spherical and non-spherical depending on the molecular geometry of the surfactant molecules. The spherical micelles have a diameter of approximately 5 nm [45].

[4]A Maxwell fluid is defined in section 3.1

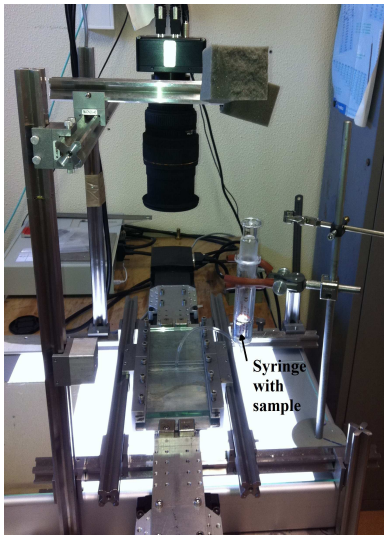

(a) *An overview of the setup.*

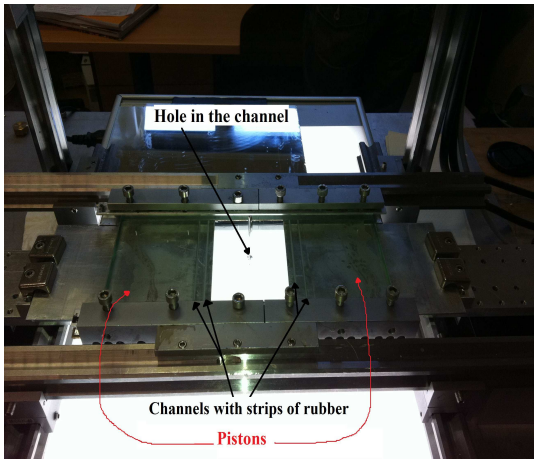

(b) *A zoom in of the pistons and channel.*

Figure 6.1: *Baudouin Saintyves' setup at CEA in Paris.*

different concentrations, since different concentrations give different phases. A concentration of for example 2 wt% Laponite will leave the clay suspension in an isotropic state, and it is possible that a transition from isotropic to nematic state can occur during an experiment. There can be done more experiments using several different velocities of the pistons, and with different temperatures of the samples, to see their influence on the ordering.

Another idea can be to build a cell with dimensions half of the dimensions to the cell used in this thesis. It is possible that it arises some disruptions and complexities because of the volume being so large in the existing cell, which will be reduced if the dimensions are reduced.

To study the speed of the tip of the finger/fracture will also be interesting to do. This can be done using the film that was recorded during the experiments. Baudouin have done this at CEA with other materials than clay suspensions, so the coding to measure the speed from the film can be gotten from him.

Appendix A

Camera settings

The settings to the camera PROSILICA GX can be changed in the program *Measurements & Automation*. On the left column, under configuration, press "Devices and Interfaces". Then press "NI-IMAQdx Devices" and then press "cam0: Allied Vision Technologies GX1050 (02-2400B)". The window should now look like the picture in figure A.1. The different settings of the camera can now be changed. Under "Acquisition" the frequency (pictures per second) can be set under "AcquisitionFrameCount". The best frequency for this camera is 50 pictures/s. The maximum frequency of this camera can be seen under "AcquisitionFrameRateLimit" and is 112.435350 pictures/s. "AcquisitionMode" is set to continuous, which means that the camera will continue to take pictures until it is asked to stop. If one wants the camera to just take a certain amount of pictures, the "AcquisitionMode" should be put to "MultiFrame", and the amount of pictures can be set under "AcquisitionFrameCount".

Under "Exposure", the exposure time can be change under "ExposureTimeAbs". A good exposure time for the experiments performed in this thesis is 1084 μs. Under "Gain" the gain can be changed. This is done under "GainRaw", and is here set to 6. This means that the value of each pixel is multiplied six times. The gain also multiplies the noise, so the gain have to be matched with the exposure time. The exposure time increases the amount of light that is let in, so the more light the better, and then the gain can be lower to reduce the noise. Some "blinking", which looks like interference can sometimes appear on the film. This can be removed by reduce the gain and increase the exposure time, or by increase the gain and reduce the exposure

time.

Under "ImageFormat" the size of the image can be changed. The size is here set to 1024 pixels in both the X-, and the Y- direction. The "PixelFormat" is set to "Mono8", which means that the image is in black and white. The rest of the settings should all be set to the default values.

To start recording with the camera, the program *Measurements & Automation* must be closed. Then open the software *labVIEW*. Here the file "GrabAvi.vi" is created to control the camera and can be seen in the figure A.2. The camera name must be set to "cam0", and then it is just to press "run" to start recording.

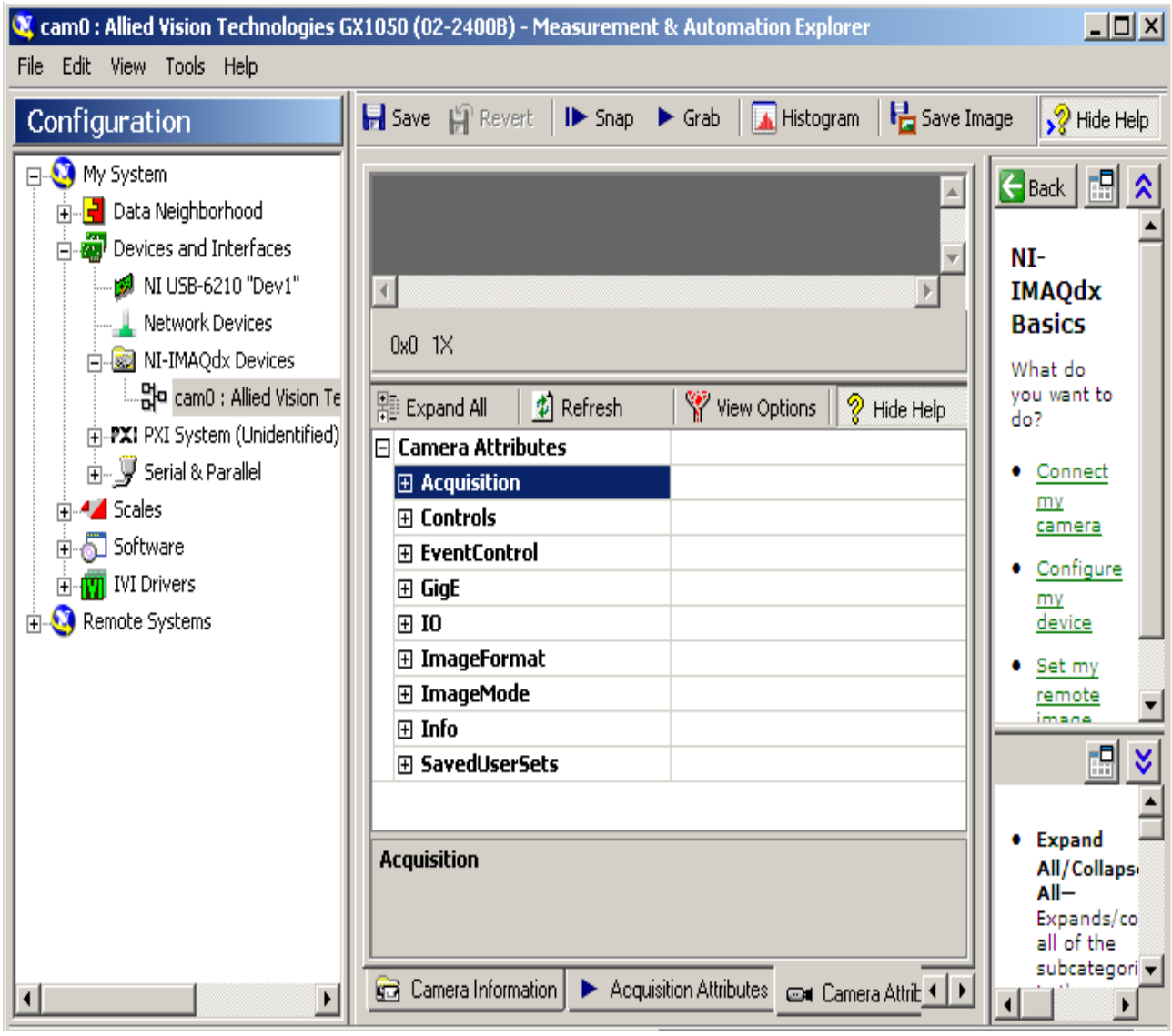

Figure A.1: *A picture of the program Measurements & Automation, used to change the camera settings.*

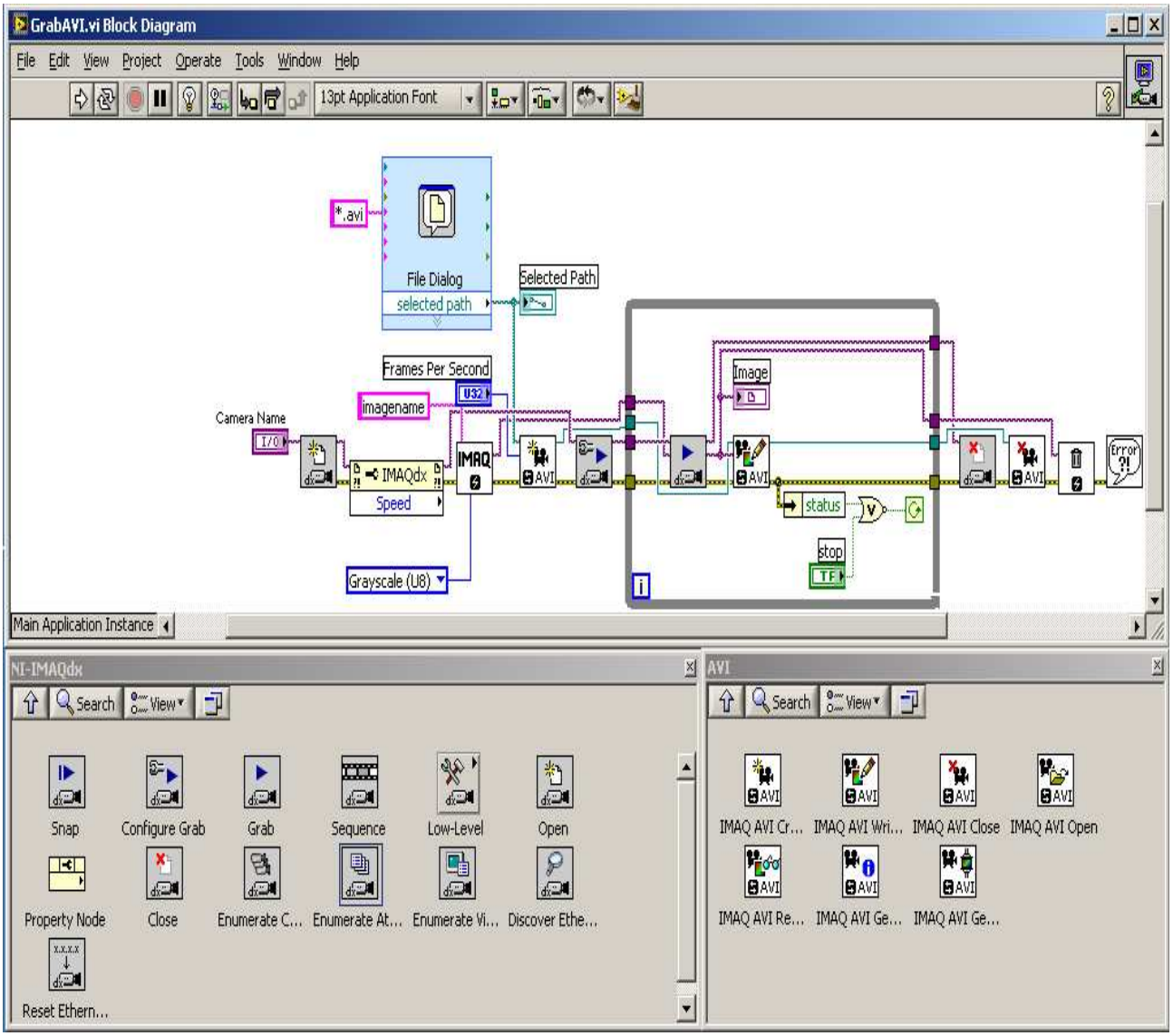

Figure A.2: *A picture of the labVIEW code to control the camera.*

Appendix B

Motor settings

The motors are controlled using the program *WinPos*, which can be seen in figure B.1. Here the velocity, acceleration and position of the pistons are set.

First the motors must be connected. This is done by pressing "Controller", and then pressing "Connect". The velocity and acceleration can be changed by pressing "Configuration", then pressing "Dyn. parameters". Here the velocity and acceleration can be set to a desirable value. The velocity is the value behind V, and the accelerations is the value behind A. The maximum velocity of the motors is 90 mm/s, but the motors are not strong enough to pull the pistons apart faster than 30 mm/s.

The distance the pistons will be pulled apart is also set in this program. When the pistons are pushed together as much as possible, press "Extras", then press "Set reference point 0" to set this position to zero. Then if the pistons shall be pulled apart, the X- and Y- value should be set to minus-values. If the X- and Y- value is set to -30, the pistons will be pulled apart a distance of 30 mm. The position of the motors can be moved both using absolute values or with relative values.

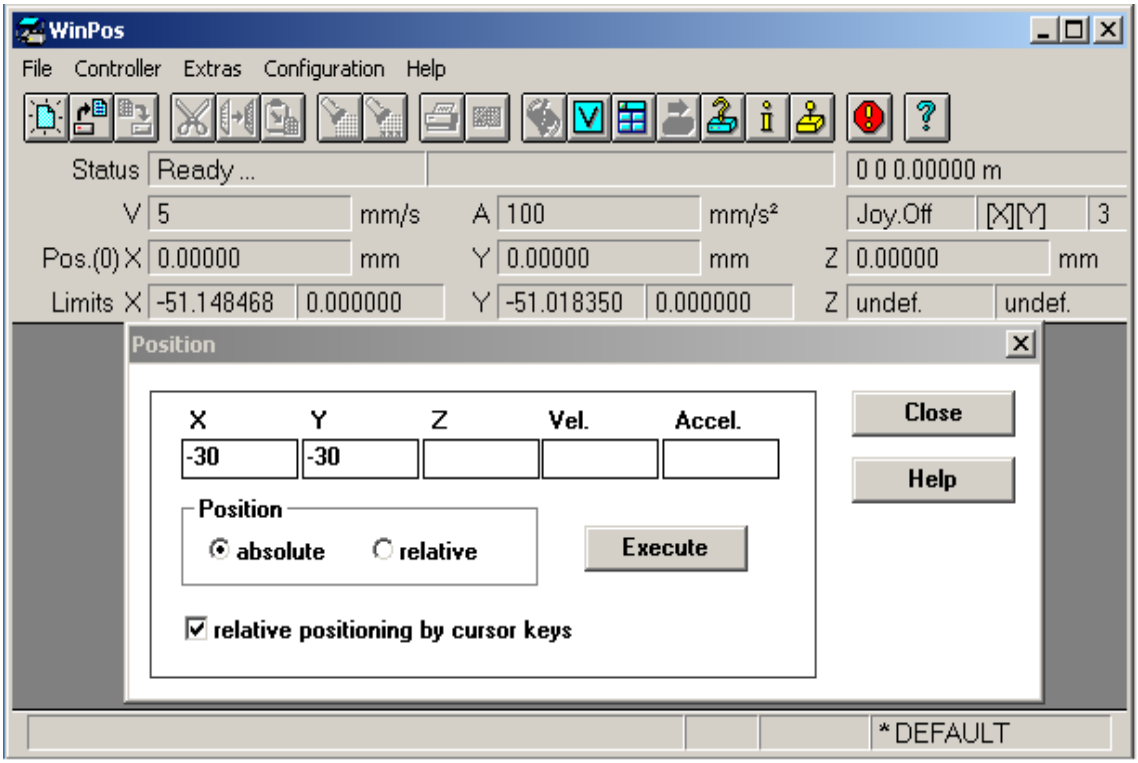

Figure B.1: *A picture of the program WinPos that controls the motors.*

Appendix C

Films of the experiments

There have been made films from all the experiments performed during the work with this thesis. Films to all the experiments with the results used in this thesis can be found with my supervisor Jon Otto Fossum.

Each film has been given a name that gives information about the experiment. Examples of filenames, and explanations to each of the parts in the names are given in the figures C.1, C.2 and C.3.

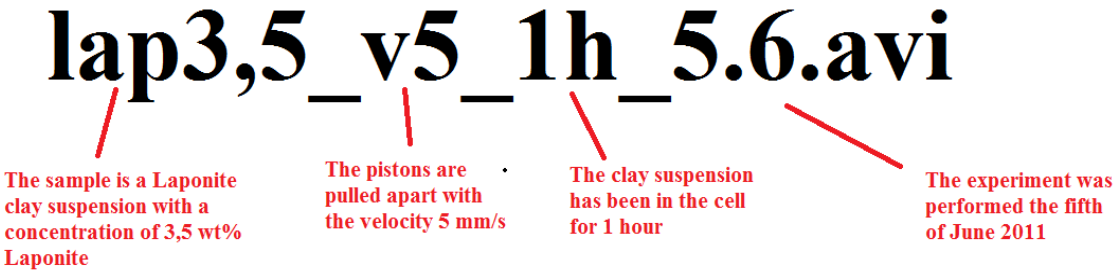

Figure C.1: *Filename to a film of an experiment with Laponite clay suspension.*

To record films of the experiments performed with crossed polarizers, a camera that can record in colors is needed. Since the PROSILICA GX camera cannot record in colors, an iPhone (cell phone) was used to record the experiments instead. Because the recording was done with a cell phone, the quality of the films from the experiments with crossed polarizers is poor.

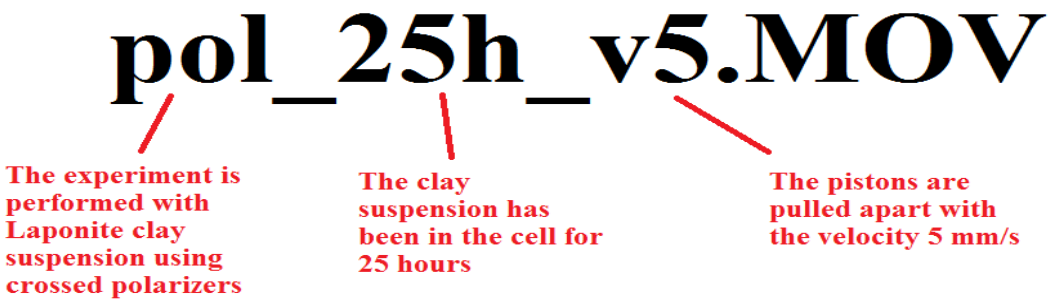

Figure C.2: *Filename to a film of an experiment with Laponite clay suspension using crossed polarizers.*

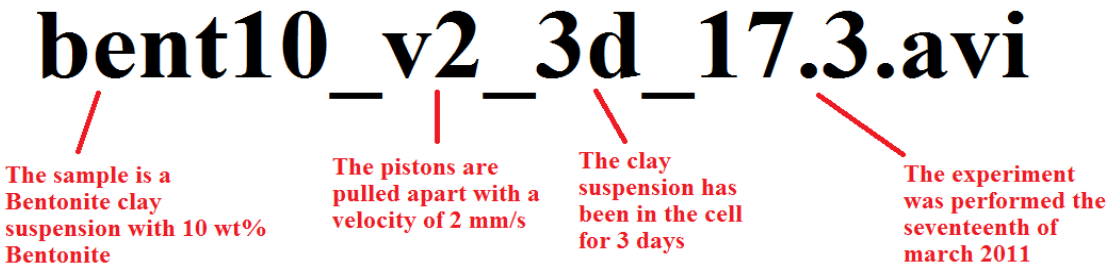

Figure C.3: *Filename to a film of an experiment with Bentonite clay suspension.*

The films are saved in folders with the names: Liquid state, Sol-gel transition state, Gel state, Bentonite experiments and Polarization experiments. In the folder "Liquid state" the experiments performed in the liquid state with clay suspension consisting of 3 wt% and 3,5 wt% Laponite and the velocities 1, 5, 10, 20, 30 and 50 mm/s are saved. It is the same for the folders "Sol-gel transition state" and "Gel state", but here the experiments are performed at the sol-gel transition state and in the gel state. In the folder "Bentonite experiments" the experiments performed in setup II using the clay suspensions with 10 wt% Bentonite are saved. There were some problems recording the films of the Bentonite experiments, so the films of the experiments with 8 wt% and 9 wt% Bentonite were lost. In the folder "Polarization experiments" the experiments performed with crossed polarizers are saved. It is one film that is named "backpol_70h_v1", this means that the pistons are pushed together again after an experiment.

Bibliography

[1] G. Schramm: *A Practical Approach to Rheology and Rheometry*, Haake Instruments Inc., (2000)

[2] G.K. Batchelor, H.K: Moffatt and M.G. Worster: *Perspectives in Fluid Dynamics, A Collective Introduction to Current Research*, (2000)

[3] H.A. Barnes, J.F. Hutton and K.Walters : *An Introduction to Rheology*, Elsevier, (1989)

[4] J.W. Dally: *Dynamic Photoelastic Studies of Fracture*, THE WILLIAM M. MURRAY LECTURE, 1979

[5] T. Vicsek: *Fractal Growth Phenomena*, World Scientific, (1989)

[6] A.B. Ryskin, H. Pleiner and H.W. Muller: *Hydrodynamic instabilities in ferronematics*, The European Physical Journal E 11, 389-397 (2003)

[7] P.G. Saffman and G. Taylor: *The penetration of a fluid into a porous medium or Hele-Shaw cell containing a more viscous liquid*, Proc. R. Soc. A 245, 312, (1958)

[8] G. J. da Silva, J. O. Fossum, E. DiMasi, K. J. Måløy and S. B. Lutnæs: *Synchrotron x-ray scattering studies of water intercalation in a layered synthetic silicate*, Physical Review E 66, 011303, (2002)

[9] F. Bergaya, B.K.G. Theng and G. Lagaly: *Handbook of Clay Science*, Elsevier Ltd., (2006)

[10] F.L.O. Paula, G.J. da Silva, R. Aquino, J. Depeyrot, J.O. Fossum, K.D. Knudsen, G. Helgesen and F.A. Tourinho: *Gravitational and magnetic separation in self-assembled clay-ferrofluid nanocomposites*, Braz. J. Phys. vol.39 no.1a São Paulo Apr. (2009)

[11] S. Jabbari-Farouji, H. Tanaka, G. H. Wegdam, and D. Bonn: *Multiple nonergodic disordered states in Laponite suspensions: A phase diagram*, Physical Review E 78, 061405, (2008)

[12] A. Mourchid, E. Lécolier, H. Van Damme, and P. Levitz: *On Viscoelastic, Birefringent, and Swelling Properties of Laponite Clay Suspensions: Revisited Phase Diagram*, Langmuir, 14, 4718-4723, (1998)

[13] L. Jyotsana and Loic Auvray: *Interaction of polymer with clays*, J. Appl. Cryst., 33:673-676, (2000)

[14] A. Mourchid, A. Delville, J. Lambard, E. Lecolier, and P. Levitz: *Phase Diagram of Colloidal Dispersions of Anisotropic Charged Particles: Equilibrium Properties, Structure, and Rheology of Laponite Suspensions*, Langmuir, 11, 1942-1950, (1995)

[15] Laponite.com, brochure: *http://www.laponite.com/pdfs/laponite.pdf*, 9 May, (2007)

[16] M. V. Kok: *A Rheological Characterization and Parametric Analysis of a Bentonite Sample*, Energy Sources, Part A: Recovery, Utilization, and Environmental Effects, 33: 4, 344 - 348, (2011)

[17] S. Abend, G. Lagaly: *Sol-gel transitions of sodium montmorillonite dispersions*, Elsevier, Applied Clay Science 16 201-227, (2000)

[18] J. C. Charmet, S. Roux, E. Guyon: *Disorder and fracture*, Cargèse, France, (1989)

[19] C. Volzone, J. O. Rinaldi, J. Ortiga: *N2 and CO2 Adsorption by TMA- and HDP-Montmorillonites*, Mat. Res. vol.5 no.4 São Carlos Oct./ Dec. (2002)

[20] W.B. Russel, D.A. Saville and W.R. Schowalter: *Colloidal Dispersions*, Cambridge University Press, (1989)

[21] F. Sallesa, I. Beurroiesb, O. Bildsteina, M. Julliena, J. Raynala, R. Denoyelb and H. Van Damme: *A calorimetric study of mesoscopic swelling and hydration sequence in solid Na-montmorillonite*, Applied Clay Science, Volume 39, Issues 3-4, Pages 186-201, (2008)

[22] F. Ziegler: *Mechanics Of Solids And Fluids*, Second edition, Springer, (1998)

[23] F. A. Holland and R. Bragg: *Fluid Flow for Chemical Engineers*, Second edition, Butterworth-Heinemann, (1995)

[24] M. Adda-Bedia and M. B. Amar: *Crack dynamics in elastic media*, Philosophical Magazine B, VOL. 78, NO. 2, 97-102, (1998)

[25] D. Bonamy and E. Bouchaud: *Failure of heterogeneous materials: A dynamic phase transition?*, Physics Reports (2010), Doi:10.1016/j.physrep.2010.07.006

[26] E. Sharon and J. Fineberg: *Confirming the continuum theory of dynamic brittle fracture for fast cracks*, Nature 397 333-335. (1999)

[27] D. Reguera, L. L. Bonilla and J. M. Rubi: *Coherent Structures in Complex Systems*, Lecture notes in physics; Vol. 567 Springer-Verlag Berlin Heidelberg (2001)

[28] P.G. Saffman: *Viscous fingering in Hele-Shaw cells*, J . Fluid Mech., vo1. 173, p p. 73-94, (1986)

[29] T. Hirata: *Fracturing due to fluid intrusion into viscoelastic materials*, Physical Review E, Volume 57, Number 2, (1998)

[30] S. Mora and M. manna: *Saffman-Taylor instability for generalized Newtonian fluids*, Physical Review E 80, 016308 (2009)

[31] E. Lemaire, P. Levitz, G. Daccord, and H. Van Damme: *From Viscous Fingering to Viscoelastic Fracturing in Colloidal Fluids*, Physical Review Letters, Volume 67, Number 15, (1991)

[32] E. Alsac, C. Laroche, E. Lemaire and H. Van Damme: *Viscochemical Fingering In A Colloidal Fluid*, Chemical Physics Letters, Volume 165, number 4, (1990)

[33] R.A. Shalliker, V.Wong, G. Guiochon: *Reproducibility of the finger pattern in viscous fingering*, Journal of Chromatography A, 1161 121-131, (2007)

[34] J.W McLean and P.G. Saffman: *The effect of surface tension on the shape of fingers in a Hele Shaw cell*, J. Fluid Mech., vol. 102, pp. 466-469, (1981)

[35] J.D. Chen and D.Wilkinson: *Pore-Scale Viscous Fingering in Porous Media* , Physical Review, Volume 55, Number 18, (1985)

[36] E. Pitt: *Penetration of fluid into a Hele-Shaw cell: the Saffman-Taylor experiment*, J. FZuid Mech., wol. 97, part 1, pp. 63-64, (1980)

[37] M. B. Amar and E. C. Poiré: *Pushing a non-Newtonian Fluid in a Hele-Shaw cell: From fingers to needles*, Physics of Fluids, Volume 11, Number 7, (1999)

[38] R. A. Schapery: *A theory of crack initiation and growth in viscoelastic media*, International Journal of Fracture, Vol. 11, No. 1, (1975)

[39] J.E. Martin and J.P Wilcoxon: *Critical Dynamics of the Sol-Gel Transition*, Physical Review, Volume 61, Number 3, (1988)

[40] M. A. Rao: *Rheology of Fluid and Semisolid Foods*, Springer Science + Business Media, LLC, Food Engineerings Series, second edition, (2007)

[41] E. Del Gado, L. De Arcangelis and A. Coniglio: *Viscoelastic Properties at the Sol-Gel Transition*, Macromol. Symp. 171, 79-86, (2001)

[42] R. Lapasin and S. Pricl: *Rheology of Industrial Polysaccharides: Theory and Applications*, Aspen Publishers, Inc, (1999)

[43] J.E. Martin, D. Adolf and J.P Wilcoxon: *Viscoelasticity near the Sol-Gel Transition*, Physical Review A, Volume 39, Number 3, (1989)

[44] A. Ponton, S. Warlus and P. Griesmar: *Rheological Study of the Sol-Gel Transition in Silica Alkoxides*, Journal of Colloid and Interface Science 249, 209 - 216 (2002), doi:10.1006/jcis.2002.8227

[45] E. Dickinson and D.J. McClements: *Advances in Food Colloids*, Blackie Academic & Professional (1995)

[46] S. L. Chin: *Fundamentals of Laser Optoelectronics*, World Scientific Publishing Co. Pte. Ltd (1989)

[47] G. Strobl: *Condensed Matter Physics*, Springer-Verlag Berlin Heidelberg (2004)

[48] S. Chandrasekhar: *Liquid Crystals*, Second edition, Cambridge University Press, (1992)

[49] T. S. El-Bawab: *Optical Switching*, Springer Science + Business Media, Inc. (2006)

[50] B. Ruzicka and E. Zaccarelli: *A fresh look at the Laponite phase diagram*, Dynamic Article Links, (2010)

[51] H. D. Young and R. A. Freedman: *University Physics with Modern Physics*, 11. edition, Pearson Education, Inc. (2004)

[52] E. L. Hansen: *Master's thesis: Colloidal Dispersions of Clay Nanoplatelets-Optical Birefringence and X-ray Studies of Nematic Phases*, Department of Physics, NTNU (2008)

[53] H. Hemmen, N. I. Ringdal, E. N. De Azevedo, M. Engelsberg, E. L. Hansen, Y. Mheust, J. O. Fossum and K. D. Knudsen: *The Isotropic-Nematic Interface in Suspensions of Na-Fluorohectorite Synthetic Clay*, Langmuir 25, 1250712515 (2009)

[54] E. Hecht: *Schaum's outline of Theory and Problems of Optics* The McGraw-Hill Companies, Inc., (1975)